Les Cahiers du GERAD ISSN: 0711–2440

Balancing realism and complexity: An accurate optimization model for electricity usage in smart homes

M.D. de Souza Dutra, M.F. Anjos
S. Le Digabel

G–2018–06

February 2018
Revised: August 2018

La publication de ces rapports de recherche est rendue possible grâce au soutien de HEC Montréal, Polytechnique Montréal, Université McGill, Université du Québec à Montréal, ainsi que du Fonds de recherche du Québec – Nature et technologies.

Dépôt légal – Bibliothèque et Archives nationales du Québec, 2018
– Bibliothèque et Archives Canada, 2018

The publication of these research reports is made possible thanks to the support of HEC Montréal, Polytechnique Montréal, McGill University, Université du Québec à Montréal, as well as the Fonds de recherche du Québec – Nature et technologies.

Legal deposit – Bibliothèque et Archives nationales du Québec, 2018
– Library and Archives Canada, 2018

GERAD HEC Montréal
3000, chemin de la Côte-Sainte-Catherine
Montréal (Québec) Canada H3T 2A7

Tél. : 514 340-6053
Téléc. : 514 340-5665
info@gerad.ca
www.gerad.ca

Balancing realism and complexity: An accurate optimization model for electricity usage in smart homes

Michael David de Souza Dutra [a,b]
Miguel F. Anjos [a,b]
Sébastien Le Digabel [a,b]

[a] *GERAD, Montréal (Québec), Canada, H3T 2A7*

[b] *Department of Mathematics and Industrial Engineering, Polytechnique Montréal (Québec) Canada, H3C 3A7*

michaeldavid.dutra@polymtl.ca
anjos@stanfordalumni.org
sebastien.le.digabel@gerad.ca

February 2018
Revised: August 2018
Les Cahiers du GERAD
G–2018–06

Abstract: Smart homes have the potential to achieve optimal energy consumption with appropriate scheduling. It is expected that 35% of households in North America and 20% in Europe will be smart homes by 2020. The control of smart appliances can be based on optimization models, which are desirable to be realist and efficient. However, from the optimization perspective, sometimes increasing realism implies a decrease in efficiency. One should make a trade-off between realism and complexity. Many of the optimization models in the literature have limitations on the types of appliances considered and/or their reliability. This paper proposes an Home Energy Management scheduling model that is accurate and efficient from the optimization perspective. Our model is an extensive appliance integrated mixed integer linear optimization model that minimizes the energy cost while keeping a given level of user comfort. Our main contribution is not only the variety of specific and accurate appliances models considered, but also their integration into a single optimization model. We consider the use of energy in appliances and electric vehicles (EV) and take into account renewable local generation, batteries, and demand-response. We propose models of a shower, a fridge and a hybrid EV that considers both the electricity consumption and the conventional fuel cost. We present computational results to validate the model and indicate how it overcomes the limitations of other models in the literature. For the instances considered in Brazil, our model gives results that, compared to the closest models in the literature, provide a cost savings in the range of 8% and 389% over a horizon of 24 hours.

Keywords: Smart home, energy management system, power demand, residential loads, multi-class appliances

Acknowledgments: This work is supported by a full scholarship from CNPq-Brazil.

1 Introduction and related work

The European Technology Platform Smart Grid in 2006 defined a smart grid to be "an electricity network integrating users, consumers, and generators in order to produce and deliver economic, secure and sustainable electricity supplies." Smart grids are used worldwide [30, 34], and many distribution companies use demand-response pricing mechanisms in the residential sector.

In the context of smart grids, the residential sector is endowed with smart homes. A smart home is a home setup where appliances and devices can be automatically controlled remotely. The number of smart homes has increased considerably in recent years. In North America the number of smart homes is expected to reach 46.2M by 2020 [42], corresponding to 35% of households. In Europe, 44.9M are expected by 2020, corresponding to 20% of households. Governments are supportive because smart homes allow investment in the grid infrastructure to be postponed. Moreover, if the local generation comes from renewables, the environmental impact of coal/oil-based generation is reduced. From the users perspective, this trend is explained by the advantages that could be explored with smart homes as: optimizing the energy usage to reduce costs while keeping a desired comfort level; selling back electricity to the utility or obtaining financial incentives from demand response programs.

In the following, let define smart home components (SHC) as the appliances, machines or technologies available to be used in a smart home. Examples of SHCs include photovoltaic panels (PVs), Wind Turbines (WTs), Combined Heating Power (CHP), Energy storage system (ESS) such batteries, heating, ventilation and air-conditioning (HVAC), Water Heating (WH). SHC are controlled by the home smart management system (HEMS), which also respects the power capacity (maximum amount of electric power that the house can use at any given time), adequate comfort level for the air/water temperature and makes decisions about the time to sell and buy electricity. In essence, an HEMS solves a scheduling problem. For details about HEMS, see [87].

There are already studies to represent this scheduling problem, see for example [69] and [11] for surveys of modeling approaches. However, existing models for the scheduling of appliances [46, 68] often do not account for the accuracy of operational and energy-consumption characteristics of each device. Table 1 summarizes the EMS models in the literature: columns 2 to 16 indicate the features included in each reference . The column *IBR constraints* indicates that the reference uses inclining blocking rates (IBR), a pricing scheme where the prices increase for each incremental block of consumption. The column *Fraction of step* indicates that the appliances can be used for brief cycles. This occurs when, for example, a model uses a fixed interval of 10 min but allows the A/C to operate in cycles of 2.5 min. The column *Comfort* indicates the model used for the comfort function, and *Pricing* indicates the pricing policy, where TOU is time-of-use and RTP is real-time pricing. Finally, the column *Objective* indicates the optimization objective(s).

Table 1 shows that no paper uses a detailed model for every appliance, i.e., an extensive appliance model. Representative appliance models give more accurate information and can better predict consumption, which is important for the evaluation of expansion strategies in the medium- and long-term [51]. Agreeing with [23] and [52], [35] affirms that *"Solving an optimization based HEMS model with high levels of accuracy based on a not enough accurate model for the controllable appliances is useless. However, there should be always a trade-off between realism and complexity"*. Finding realistic optimal approaches to smart home scheduling requires accurate and appropriate appliance models [52], which is the motivation of this paper. Even though load scheduling is a topic studied by several authors, our work proposes a distinct way to deal with the problem focusing on the trade-off aforementioned. This paper focuses in that trade-off by proposing a HEM scheduling model that is accurate, efficient from optimization perspective to minimize users' cost. Our main contribution is in combining all of the SHC mentioned at Table 1 in a single HEM system formulated in a mixed integer linear optimization problem. In summary, our contributions are as follows:

1. We propose an extensive appliance integrated linear optimization model that finds an optimal cost keeping a high level of user comfort.
2. We formulate a fridge model by linearizing a nonlinear model true to reality, maintaining fidelity and reducing complexity.

3. In some countries, for instance Brazil, the electrical shower is one of the biggest contributors to electricity bill. We propose a shower model.
4. Although the literature proposes EV models, to the best of our knowledge, no previous work has considered the additional costs of fuel or electricity recharge outside the house, which is important to the householder budget. We propose a new EV model that includes this characteristic.

The rest of this paper is organized as follows. In Section 2, we introduce the models for the appliances, IBR pricing, thermal machines, and other components. Section 3 describes our instances, and Section 4 presents the results. Section 5 provides concluding remarks.

2 Mathematical models

In this section, we describe the models for SHC and the integrated optimization model. Note that we consider only power consumption, and that we keep the units from references as they were published. Nomenclature is available in Appendix.

2.1 PV and solar collector

The PV and solar collector models calculate the values of the parameters E^t_{pv} and T^t_{in}. We first need to estimate T^t_o so we can use the formulas from [4, Example 9, Section 14.12]. We also need to know the quantity of solar radiation available at the surfaces of the panels and collectors. We used the equations from [29, Chapter 1,2] (without shading and "track moving" but with "clear sky"). We implemented four models: the isotropic diffuse model, HDRK model, Perez model, and the ASHRAE revised clear sky model ("Tau Model") from [4, Chapter 14] and [5, Chapter 35]. From these we selected the Perez model. We also considered the absorptance effect.

We must convert the solar radiation into power for the PV and heat for the solar collector. For the PV, we use the approach from [58] with $V = V_{mp}$; we replace Equation 3 of [58] by Equation 9 of [24]. For the cell temperature, we use the approach from [29, Section 23.3]. For the solar collector, we use the collector-efficiency equations from [29, Chapters 3–6] with the factor F' = 0.8, the temperature of the plates equal to the outside temperature, the temperature difference between the plates and glass set to 20^{o}C, all the layers of glass having the same temperature, and the inlet water comes from the street.

2.2 Wind turbines

The wind turbine (WT) model forecasts the value of E^t_{wt}. Villaneuva & Feijóo [81] propose a relationship between wind speed and WT power produced. They consider operation at maximum capacity and specify cut-in and cut-out inequalities. We have slightly modified their strict inequalities to include the end-points:

$$\begin{array}{cc} \text{Wind speed interval (m/s)} & \text{Output power (W)} \\ U < U_{CutIn} & 0 \\ U_{CutIn} \leq U < U_{Pmax} & 0.5 A\rho U^3 C_{p2} \\ U_{Pmax} \leq U \leq U_{CutOut} & Pmax \\ U > U_{CutOut} & 0 \end{array} \tag{1}$$

where U is the wind speed (m/s); U_{CutIn} is the lowest wind speed (m/s) at which it is possible to obtain power from the wind; U_{Pmax} is the wind turbine power speed rate (m/s); A is the area of the air-stream, measured in a perpendicular plane to the direction of the wind speed (m^2); ρ is the air density (kg.m^{-3}); C_{p2} is the power coefficient, which is the ratio between the power produced by the WT and the power carried by the free air-stream; U_{CutOut} is the upper limit (m/s) at which it is possible to get power from the wind; and $Pmax$ is the rated power (W).

Table 1: Summary of features of EMS models

Reference	Wind Turbine	PV	Solar Collector	ESS	Water Heater	Shower	Freezer/Fridge	HVAC	Phase Machines	A_{IEUI}	EV	CHP	Lighting	IBR Constraints	Fraction of Step	Comfort	Pricing	Objective
Our	x	x	x	x	x	x	x	x	x	x	x	x		x	x	L	TOU	↓ D vs C
[85]								x							x	Q	NC	↓ TD
[84]													x			L		↓ IL
[83]				x					x	x						Q	NC	↓ C vs D vs B
[25]								x	x	x						Q	DA RTP	↓ D vs C
[44]									x	x							DA RTP	↓ C
[28]					x											L	DA TOU	↓ B
[40]								x								L	DA NC	↓ B vs D
[64]									x	x						CF	NC RTP	↑ -D vs C
[41]				x				x	x	x		x				L	DA NC	↓ C
[89]									x	x				x		L	NC	↓ C vs WT
[9]	x	x		x												L		↓ C
[61]					x			x								L	NC	↑ -D vs C
[62]					x			x								L	NC	↑ -D vs C
[53]									x	x				x		L	RTP	↓ C vs WT
[33]									x	x							RTP, TOU	↓ C
[65]				x						x	x					L	TOU	↓ C / ↓ C vs D
[18]				x										x			NC	↓ C
[37]										x							DA TOU	↓ C
[1]									x	x						L	NC	↓ C / ↓ C vs PL
[2]				x					x	x							DA RTP	↓ C
[7]	x	x		x	x			x	x	x		x				NL	RTP	many
[8]				x	x			x	x	x		x				NL	RTP	many
[3]				x				x	x	x						L	NC	↓ C vs D
[19]					x			x	x	x	x						RTP	↓ B
[88]				x	x			x		x	x						RTP	↓ C
[82]					x					x							NC	↓ C
[57]			x		x			x	x	x	x					L	RTP	↓ C
[67]					x		x	x									TOU	↓ C
[17]								x	x	x						L	NC	↓ C
[68]					x		x	x		x						NL	TOU	↑ -D vs C
[49]		x		x							x							↓ C
[54]		x		x													Flat	↓ C vs CO_2
[79]		x		x							x							↓ E[C]
[36]		x		x						x	x							↓ C
[75]	x			x					x	x						L	RTP	↓ C
[35]		x		x	x						x			x		–	TOU,RTP	↓ C
[71]		x		x			x	x									TOU	↓ C vs D
[52]		x		x					x	x	x						NC	↓ C
[70]	x	x		x				x		x	x						NC	↑ Profit
[55]				x				x		x							NC	↓ C
[32]		x		x							x						NC	↓ C
[60]		x		x	x			x	x		x						NC	↓ C
[74]	x	x		x	x		x	x		x		x	x			L	RTP	↓ C
[73]	x	x		x	x		x	x		x		x	x			L	RTP	↓ C / ↓ C vs PL
[45]				x	x		x	x		x	x	x					TOU	↓ C

Legend: ↓: Minimize ↑: Maximize IL: Illumination level D: Discomfort -D: Comfort C: Cost L: Linear
Q: Quadratic NC: Not constant TD: Thermal discomfort B: Electricity bill BL: Battery loss
DA: Day ahead CF: concave function WT: Waiting time NL: Nonlinear PL: Peak load

The Weibull probability distribution function (PDF) of U at a specified location is

$$f_U(U) = \left\{ \begin{array}{ll} \frac{k}{C}(\frac{U}{C})^{k-1}e^{-(U/C)^k}, & U \geq 0 \\ 0, & U < 0 \end{array} \right\},$$ where k is a shape parameter and C is a scale parameter [81].

We can find ρ using the ideal gas law for dry air, Equation 1.18 from [78]: $\rho = \frac{p}{RT}$, where p is the absolute pressure (101.325 kPa), T is the temperature (K), and R is the specific gas constant for dry air (287.058 $\frac{J}{kg.K}$).

2.3 Heating, ventilation, and air conditioning (HVAC)

Having $\frac{\Delta t_2}{V_{house}\rho_{air}c_{air}} = \Upsilon$, the HVAC model is given by constraints (2) to (14).

$$T_{room}^{t+1} = T_{room}^{t} + \Upsilon[3600(P_{heating}z_{HVAC}^{t} - P_{cool}z_{air}^{t})] + \Upsilon(G^{t}) \qquad \forall\, t \in T/\{|T|\} \tag{2}$$

$$G^{t} = \left[\frac{A_{ceiling}}{R_{ceiling}} + \frac{A_{wall}}{R_{wall}} + \frac{A_{window}}{R_{window}}\right](T_o^t - T_{room}^t) + [n_{ac}V_{house}\rho_{air}c_{air}](T_o^t - T_{room}^t) + 3600H_p^t + 3600(SHGC)A_{window}H_{sun}^t \forall\, t \in T/\{|T|\} \tag{3}$$

$$T_{room}^1 = T_o^1 \tag{4}$$

$$y_{HVAC}^t \in \{0,1\} \qquad \forall\, t \in T \tag{5}$$

$$y_{air}^t \in \{0,1\} \qquad \forall\, t \in T \tag{6}$$

$$x_{HVAC}^t = P_{heating}z_{HVAC}^t + P_{cool}z_{air}^t \qquad \forall\, t \in T \tag{7}$$

$$1 \geq y_{HVAC}^t + y_{air}^t \qquad \forall\, t \in T \tag{8}$$

$$z_{HVAC}^t \leq y_{HVAC}^t \qquad \forall\, t \in T \tag{9}$$

$$z_{air}^t \leq y_{air}^t \qquad \forall\, t \in T \tag{10}$$

$$z_{HVAC}^t \geq 0 \qquad \forall\, t \in T \tag{11}$$

$$z_{air}^t \geq 0 \qquad \forall\, t \in T \tag{12}$$

$$V_{HVAC}^t \geq T_{room}^t - T_f^t \qquad \forall\, t \in D_{air} \tag{13}$$

$$V_{HVAC}^t \geq -T_{room}^t + T_f^t \qquad \forall\, t \in D_{air} \tag{14}$$

Constraints (2) to (12) represent the room temperature, and (13) and (14) permit deviation and count the discomfort from the target temperature during the intervals when the user needs the HVAC.

The constraints (2) and (3) are based in Shao et al. [72]. They propose a model with a 1.2% total daily energy difference. The differences between our model and their model is explained forward.

Assumptions: A_{wall} in [72] is derived from floor area assuming that the height of the house is 10 ft. If A_{wall} is not given by the user, we assume that the floor is square and calculate A_{wall} accordingly. In [72] there is a consideration of a specific window turned to south. In our model, we consider every window of same type. The values for H_p^t, SHCG and n_{ac} are not availavble in [72]. H_p can be found ([7], [86, pp. 41–43]) via $H_p = P_{activity}A_{body}$, where $P_{activity}$ is the metabolic rate and $A_{body} = 0.202m^{0.425}h^{0.725}$, where m is the mass of the body (kg), and h is the height (m). We define np^t to be the number of occupants at time t. H_p is then given by:

$$H_p^t = \sum_{i=1}^{np^t} P_{activity,i}^t A_{body,i}^t \qquad \forall\, t \in T.$$

For SHCG, we used the average of the values of [4, p. 353]. H_{solar} is calculated from our PV model. We now discuss the calculation of n_{ac}. We first note that the infiltration loss in [72], $\frac{\Delta_t}{\Delta_c}(\frac{11.77Btu}{^oF\times ft^3}n_{ac}V_{house})(T_o^t - T_{room}^t)$, is large ($\Delta_c$ is the energy (Btu) needed to change the air temperature by 1^{o}F). Therefore, we assume that the term $\frac{11.77Btu}{^oF\times ft^3}$ should be multiplied by 10^{-3}. If we consider the infiltration formula $\frac{\Delta_t}{\Delta_c}(n_{ac}V_{house}\rho C_{air})(T_o^t - T_{room}^t)$ where ρ is the air density, we see that $\frac{11.77Btu}{^oF\times ft^3}$ replaces ρC_{air} in the formula. For $\rho = 1.2$ and $C_{air} = \frac{1012J}{kg^oC}$, we have $\rho C_{air} = \frac{1214.4J}{^oC\times m^3} \approx \frac{0.018Btu}{^oF\times ft^3}$. That value matches the formula from [4, Chapter 17] : $n_{ac} = ACH = \frac{3.6Q_i}{V}$, $Q_i = A_L IDF$, $A_L = A_{es}A_{ul}$, where ACH is the air changes per hour; Q_i is the infiltration airflow rate (L/s); V is the building volume (m^3); A_L is the building effective leakage area (cm^2) (including the flue) at a reference pressure difference of 4 Pa, assuming a discharge coefficient CD of 1; IDF is the infiltration driving force $(L/(s.cm^2))$; A_{es} is the building exposed surface area (m^2); and

A_{ul} is the unit leakage area ($\mathrm{cm}^2/\mathrm{m}^2$). This gives $ACH = \frac{3.6A_{es}A_{ul}IDF}{V}$. With the values given for IDF [4, Table 5 of Chapter 17] and A_{ul} [4, Table 3 of Chapter 17], n_{ac} has an acceptable value.

Our other assumptions are as follows: i) there is a single conditioned space; ii) no independent thermal storage is coupled to the main heating/cooling equipment; iii) the control of humidity is neglected; iv) internal heat sources of the equipment are neglected; v) the temperature is constant throughout the space.

We have rewritten the model from [72] with the considerations above to arrive at an on-off model composed of constraints (2) to (8), (13), and (14).

Flexibility: (2) introduces the on-off feature, since y^t_{HVAC} and y^t_{air} are binary variables. Thus, we are working with fixed power in a fixed time interval. However, forcing a machine to operate for a full interval could generate an overcharge. We therefore introduce the variable z^t_a to allow appliances to operate for shorter periods. Let z^t_a be the fraction of Δ_t during which appliance a is on. We have $z^t_a y^t_a = z^t_a$. If $y^t_a = 1$ then $0 \le z^t_a \le 1$; if $y^t_a = 0$ then $z^t_a = 0$. We can model the implications with inequalities such as (9) and (10). Therefore, with the new variable, we can build a single model that is represented by constraints (2) to (14). With the objective function (146), we can, without any impact on the results, drop the variables y^t_{HVAC} and y^t_{air} and the restrictions (5) and (8) to (10). We refer to this as the *Fraction of step*.

The strategy above does not indicate when the machine is on/off in the fixed time interval. Given x^t_{HVAC} for each $t \in T$, we can find whether the machine is on or off at each second.

The temperature at the end of the period depends on exactly when it is used. If it is used at the end of the period, the results are closer to the results for the complete optimization model. However, the difference is not so high. With nomila power of 25 kW, the difference in temperature will be around 0.12^{o}C at some point inside the time interval.

It is worth to mention that the addition of z^t_a does not violate energy conservation. For example, suppose an appliance has a power of 5000 W and it operates for 50% of the time, giving a consumption of $5000\,W \times 0.5\Delta_t$. It will contribute $2500\,W \times \Delta_t$ to the conservation constraint.

2.4 Water heaters

Having $\frac{\Delta t_2}{(v_{tank}C_p)} = \Psi$, the HVAC model is given by constraints (15) to (21).

$$T^{t+1}_{out,wh} = T^t_{out,wh} + \Psi[-227.4 fr^t_{wh} C_p (T^t_{out,wh} - T^t_{in})] + \Psi[3600(x^t_{wh} + 1000 P^t_{CHPt})] - \Psi[3600(UA)_{wh}(T^t_{out,wh} - T^t_{room})] \;\forall\, t \in T/\{|T|\} \quad (15)$$

$$T^1_{out,wh} = T^1_{in} \quad (16)$$

$$x^t_{wh} = P_{wh} y^t_{wh} \qquad \forall\, t \in T \quad (17)$$

$$y^t_{wh} \in \{0,1\} \qquad \forall\, t \in T \quad (18)$$

$$V^t_{wh} \ge T^{wh}_f - T^t_{out,wh} \qquad \forall\, t \in D_{wh} \quad (19)$$

$$V^t_{wh} \ge -T^{wh}_f + T^t_{out,wh} \qquad \forall\, t \in D_{wh} \quad (20)$$

$$y^t_{wh} \le E_{wh} \qquad \forall\, t \in T \quad (21)$$

Constraints (15) to (18) represent the water heating temperature, and (19) and (20) permit deviation and count the discomfort from the target temperature during the intervals when the user needs hot water. If $E_{wh} = 0$, there is no water heater (WH), $T^t_{out,wh}$ is at most the street water temperature or the water temperature coming from SC if it exists; Constraint (21) is then needed, which also imposes an upper bound on the temperature. Note that T^t_{room}, in (15), comes from the HVAC model.

The model was constructed from [29, Equation 8.3.3] and validated by comparing with the model from [72], which was validated with experiments in the reality.

For a validation example, we convert units where necessary and use the data: room temperature given in Figure 1, $T^1_{out,wh} = 77^oF$, $x^t_{wh} = 5\,\mathrm{kW}\ \forall\, t \in T$, the surface area of the WH equals $5\,\mathrm{ft}^2$, the tank heat resistance equals $25^oF \cdot ft^2 \cdot h/Btu$, $\Delta_t = 10\,\text{min}$, $T_{in}^t = 104^oF\ \forall\ t \in T$, $v_{tank} = 80\,\text{gallons}$, $fr_{wh}^t = \ddot{f}\ \forall\ t \in T$ (gallons/min) for $\ddot{f} \in \{0, 1, 5, 10\}\ \forall\ i$. If we assume that the WH is always on, we obtain the results of [72] when $fr_{wh}^t > 0\ \forall\ t \in T$, as shown in Figures 2 and 3. When $fr_{wh}^t = 0\ \forall\ t \in T$, the model deviates after about 150^oC, but in practice there are mechanisms to avoid water evaporation. Thus, our model is faithful to the results of [72].

2.5 Shower

The shower is modeled by constraints (22) to (29).

$$T_{chu\_hand}^t \leq T_{out,wh}^t \qquad \forall\ t \in D_{chu} \tag{22}$$
$$T_{chu\_hand}^t \geq T_{inlet}^t \qquad \forall\ t \in D_{chu} \tag{23}$$
$$T_{out,chu}^t = T_{chu\_hand}^t + \frac{60x_{chu}^t}{C_e fr_{chu}^t} \qquad \forall\ t \in D_{chu} \tag{24}$$
$$x_{chu}^t = P_{chu} y_{chu,hot}^t \qquad \forall\ t \in D_{chu} \tag{25}$$
$$x_{chu}^t = 0 \qquad \forall\ t \notin D_{chu} \tag{26}$$
$$V_{chu}^t \geq T_f^{chu} - T_{out,chu}^t \qquad \forall\ t \in D_{chu} \tag{27}$$
$$V_{chu}^t \geq -T_f^{chu} + T_{out,chu}^t \qquad \forall\ t \in D_{chu} \tag{28}$$
$$y_{chu,hot}^t \in \{0,1\} \qquad \forall\ t \in D_{chu} \tag{29}$$

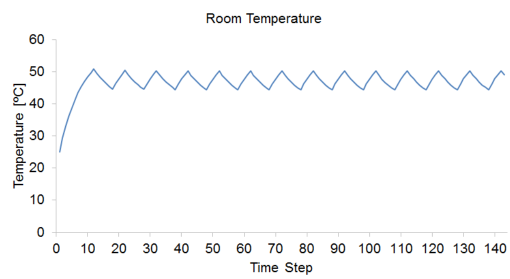

Figure 1: Room temperature for validation example.

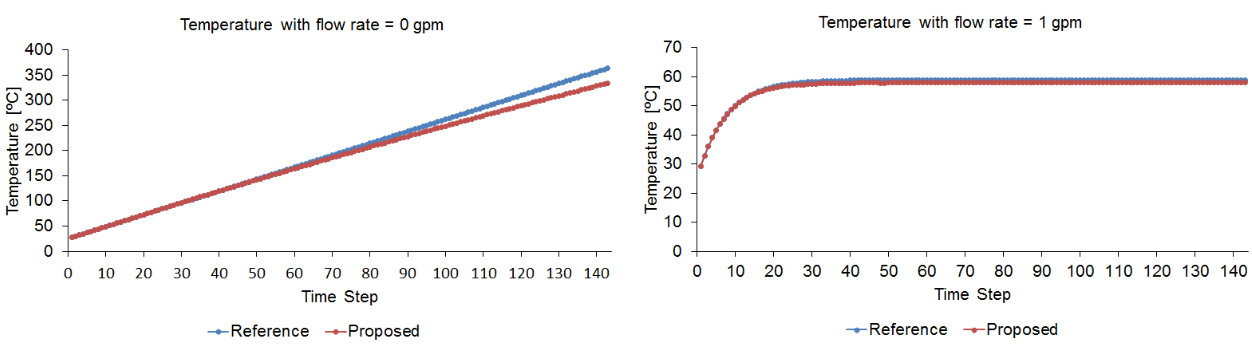

Figure 2: Comparison of our model and reference model from [72]: WH always on and low flow rate.

We assume that all the water inside the WH is at the same temperature. The *Fraction of step* idea can be applied by relaxing y_{wt}^t.

Constraints (22) and (23) place bounds on the shower temperature without using the shower resistance. Constraints (24) to (26) represent the shower temperature, and (27) and (28) permit deviation and count the discomfort from the target temperature during the intervals when the user needs the shower. Constraints (29) are the binary restrictions.

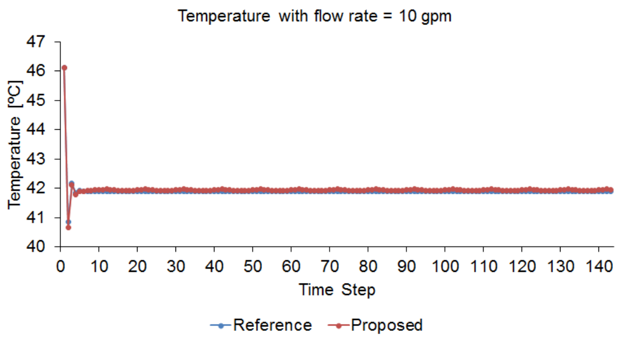

Figure 3: Comparison of our model and reference model from [72]: WH always on and high flow rate.

We obtain model (22) to (29) from [86, Chapter 1] through the thermodynamics formula $\dot{Q} = \dot{m}C_p\Delta T$ where $\dot{m}$ is the mass flow rate of a fluid flowing in a pipe (kg/s); C_p is the specific heat of the fluid (J/kg$\cdot^o C$); ΔT is the temperature difference ($^o C$) and $\dot{Q}$ is the rate of net heat transfer into or out of the control volume (W). Moreover, $\dot{m} = \rho V A_c$ where ρ is the fluid density; V is the average fluid velocity in the flow direction; and A_c is the cross-sectional area of the pipe or duct. This gives $\dot{Q} = \rho\dot{V}C_p\Delta T$, where $\dot{V}$ is the volumetric flow rate (m^3/s). We write $P = \rho\dot{V}C_p\Delta T$ where P is the power (W) lost or injected.

For each step $t \in D_{chu}$, $P_{chu} = P$, f_r is the equivalent measure of $\dot{V}$ (gpm) and $\Delta T = T_{out,chu} - T_{chu\_hand}$. This gives (24) and (25). The *Fraction of step* idea can be applied by relaxing $y^t_{chu,hot}$.

2.6 Batteries (ESS)

ESS is modeled by constraints (30) to (41).

$$SOC^{t+1} = SOC^t + \frac{100\Delta t_2}{E_{bat}}\left(P^{ch,t}_{bat}\eta^{ch}\mu - \frac{P^{dch,t}_{bat}}{\eta^{dch}\mu} - p_{loss}y^t_{float}\right) \quad \forall\ t \in T\backslash\{|T|\} \tag{30}$$

$$SOC^t \geq SOC_{min} \quad \forall\ t \in T \tag{31}$$

$$SOC^t \leq SOC_{max} + (100 - SOC_{max})y^t_{float} \quad \forall\ t \in T \tag{32}$$

$$SOC^1 = SOC_{min} \tag{33}$$

$$P^{ch,t}_{bat} \leq \frac{P^{ch}_{max}}{\eta^{ch}\mu}y^{ch,t}_{bat} \quad \forall\ t \in T \tag{34}$$

$$P^{ch,t}_{bat} \geq \frac{P^{ch}_{min}}{\eta^{ch}\mu}y^{ch,t}_{bat} \quad \forall\ t \in T \tag{35}$$

$$P^{dch,t}_{bat} \leq P^{dch}_{max}\eta^{dch}\mu y^{dch,t}_{bat} \quad \forall\ t \in T \tag{36}$$

$$P^{dch,t}_{bat} \geq P^{dch}_{min}\eta^{dch}\mu y^{dch,t}_{bat} \quad \forall\ t \in T \tag{37}$$

$$1 \geq y^{dch,t}_{bat} + y^{ch,t}_{bat} \quad \forall\ t \in T \tag{38}$$

$$y^{dch,t}_{bat} \in \{0,1\} \quad \forall\ t \in T \tag{39}$$

$$y^{ch,t}_{bat} \in \{0,1\} \quad \forall\ t \in T \tag{40}$$

$$y^t_{float} \geq 0 \quad \forall\ t \in T \tag{41}$$

Constraints (30) establish the relationships between the state of charge (SOC), discharging and charging powers, and battery float losses. Constraints (31) place a lower bound on the SOC. Constraints (32) place an upper bound on the float losses that is activated when a threshold is reached. Constraints (33) set an initial value for the SOC. Constraints (34) to (37) set bounds on the discharging and charging power. Constraints (38) ensure that at each $t \in T$ the battery either charges or discharges. Constraints (39) to (41) are the binary restrictions.

We based our model on [7], [8], and [88]. The differences between these models will be explained using the following data: $|T| = 144$, $E_{bat} = 24\,\text{kWh}$, $SOC_{max} = 80\%$, $SOC_{min} = 20\%$, $P^{ch}_{max} = P^{dch}_{max} = 3.3\,\text{kW}$, $P^{ch}_{min} = P^{dch}_{min} = 0.3\,\text{kW}$, $\eta^{ch} = \eta^{dch} = 0.91$, and $\mu = 1$. We define the objective function as $\max 30SOC^2 - \sum_{t\in T} SOC^t$. Thus, in interval 1, the battery will charge at a maximal power and in interval 2 it will discharge at a maximal power: see Figure 4. Energy is given by $\Delta_t \times Power$, so we show only power in the energy flow in Figures 4 and 5.

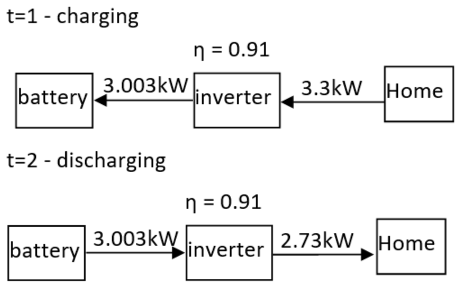

Figure 4: Solutions of battery model.

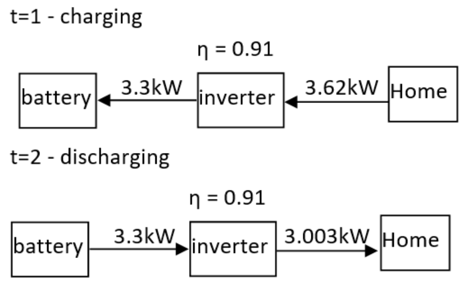

Figure 5: Solutions of battery model.

The solution to the models of [7] and [8] is $SOC^2 = 22.0854$, $SOC^t = 20\ \forall\ t \in T\backslash\{2\}$, $P^{ch,1}_{batt} = P^{dch,2}_{batt} = 3.003$, and the other power variables are null. Thus, the charging consumption was 3.003 KW instead of 3.3 KW. For the discharging, $P^{dch,2}_{batt}$ takes the value of the power inside the battery instead of the power sent to the house. Thus, when we put these variables into the energy conservation constraints, they use different values than the values sent to or consumed in the battery model. Therefore, there is a energy construction if we take the home as the reference point.

The model from [88] gives the same objective value, but it reproduces exactly the process shown in Figure 4. However, we could have maximal power charging in the battery, as shown in Figure 5.

Our model implements the energy flow shown in Figure 5,which gives a better objective value.

We also consider the battery float charge loss. According to [15], the global loss is given by $L_{Bat} = L_{Bat,eff} + E_{Float}$, where $L_{Bat,eff}$ is the energy efficiency loss, represented in our model by μ; and E_{Float} is the battery float charge loss, which results from the energy used to maintain the battery charge when SOC $\approx$ 100%. Constraints (32) implement this. The *Fraction of step* idea can be applied by relaxing the binaries variables.

2.7 Fridge

Fridge is modeled by constraints (42) to (52).

$$T^{t+1}_{freezer} = T^t_{freezer} - \frac{7\Delta t}{25} y^t_{comp} + \frac{15\Delta t}{67}\left(1 - y^t_{comp}\right) \qquad \forall\ t \in T\backslash\{|T|\} \tag{42}$$

$$T^{t+1}_{refri} = T^t_{refri} - 0.1467\Delta t y^t_{comp} + 0.1196\Delta t(1 - y^t_{comp}) \qquad \forall\ t \in T\backslash\{|T|\} \tag{43}$$

$$T^1_{freezer} = T^{start}_{freezer} \tag{44}$$

$$T^1_{refri} = T^{start}_{refri} \tag{45}$$

$$x^t_{refri} = P_{comp} y^t_{comp} \qquad \forall\ t \in T \tag{46}$$

$$x^t_{freezer} = 0 \qquad \forall\ t \in T \tag{47}$$

$$V^t_{freezer} \geq T^{freezer}_f - T^t_{freezer} \qquad \forall\ t \in T \tag{48}$$

$$V^t_{freezer} \geq 0 \qquad \forall\ t \in T \tag{49}$$

$$V^t_{refri} \geq T^{refri}_f - T^t_{refri} \qquad \forall\ t \in T \tag{50}$$

$$V^t_{refri} \geq 0 \qquad \forall\ t \in T \tag{51}$$

$$y^t_{comp} \in \{0, 1\} \qquad \forall\ t \in T \tag{52}$$

We consider a frost-free top mount refrigerator. Constraints (42) and (43) represent the freezer temperature and the fridge temperature, respectively. Constraint (44) establishes the initial freezer temperature, and Constraint (45) establishes the initial fridge temperature. Constraints (46) initialize the x^t_{refri} values for the link with the complete model. Constraints (47) set $x^t_{freezer} = 0$ because the freezer temperature depends on the fridge temperature. Constraints (48) to (51) permit deviation and count the discomfort from the target temperature, and Constraints (52) are the binary restrictions.

A transient model has been developed [13, 12] for the temperatures of refrigerated compartments; the predicted energy consumption has a maximum deviation of $\pm 2\%$. Our model is based on this, with some adjustments. We observe a correlation between the power consumption and the air temperature at the evaporator outlet [12, Figures 2.15 and 2.16]. We apply Newton's law of cooling to find the temperature at the evaporator outlet when the compressor is operating. When it is off, we have a choice of two approaches. In the first, as suggested by the author via email correspondence, we assume that the temperature at the evaporator outlet is the same as the air temperature at the evaporator inlet: $T^t_{o,e} = T_{newton} y^t_{comp} + (rT^{t-1}_{freezer} + (1-r)T^{t-1}_{refri})(1 - y^t_{comp})$, where $T^t_{o,e}$ is the temperature at the evaporator outlet; T_{newton} is the temperature obtained from Newton's law of cooling; and r is the air mass fraction supplied to the freezer. In the second approach, we use Newton's law of cooling for the temperature increase around the evaporator outlet: $T^t_{o,e} = T_{newton} y^t_{comp} + T_{newton_2}(1 - y^t_{comp})$. Figure 6 compares these approaches with the reference values calculated using the equations from [12] and experimental data provided by email by the authors. We selected the approach 2.

We can rewrite Equation 3.71 from [12] as $(T^t_{o,e})' = T^t_{o,e} + \frac{3600 w_{fan}}{\dot{m}_a C_{p,a}} y^t_{comp}$, where $(T^t_{o,e})'$ is the air temperature of the fan discharge (^oC); w_{fan} is the rated fan power (W); $\dot{m}_a$ is the total mass flow rate of air (kg/h); and $C_{p,a}$ is the specific heat at a constant pressure (J/kg^oC). The fan is on only when the compressor is on.

With $\kappa \in \{T_{newton_2}, rT^{t-1}_{freezer} + (1-r)T^{t-1}_{refri}\}$ and following [12], we can write the above equations as (148) and (149) where $T^t_{eq,f}$ ($T^t_{eq,r}$) is associated with the steady-state temperature of the freezer (fridge) if constant conditions are maintained at time t (^oC); UA_f (UA_r) is the global freezer (fridge) thermal conductance (W/^oC); $\dot{m}_{d,f}$ ($\dot{m}_{d,r}$) is the air flow leaving the freezer (fridge) when the door is open; T^t_a is the exterior temperature around the fridge at time t (^oC); UA_m is the global mullion thermal conductance (W/^oC); $T^t_f = T^t_{freezer}\ \forall\, t \in T$; and $T^t_r = T^t_{refri}\ \forall\, t \in T$. Note that T^t_a is T^t_{room} from the HVAC model. Using these equations, we obtain $\forall\, t \in \{1, ..., T-1\}$, $\forall * \in \{r, f\}$:

$$T^{t+1}_* = T^t_{eq,*} - (T^t_{eq,*} - T^t_*) e^{[-\frac{60\Delta_t (Ua_* + UA_m + \frac{\dot{m}_* C_{air}}{3600} y^t_{comp})}{C_*}]}.$$

Figures 7 and 8 compare the results from these equations with experimental results and the reference model [12, Condition 3], assuming standard masses in the enclosure thermocouples and a fixed air density.

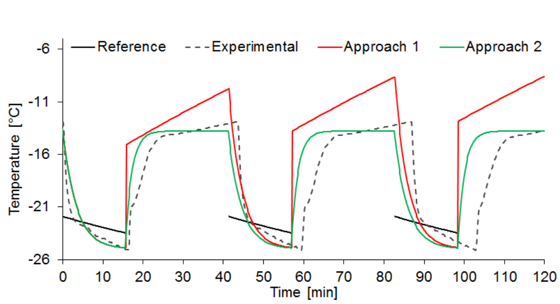

Figure 6: Comparison of ways to find $T^t_{o,e}$.

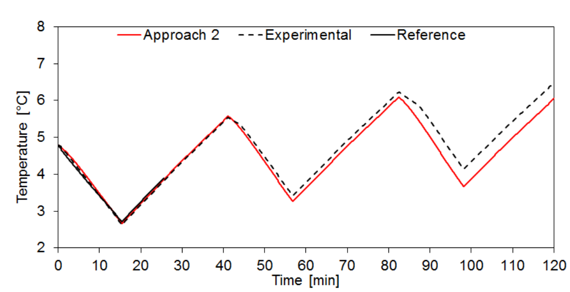

Figure 7: Our results compared to experimental results and reference model from [12] (fridge temperature).

This model is nonlinear and will increase the complexity of our optimization model. For simplicity, we perform a linear regression, obtaining:

$$\begin{aligned} T^t_f &= \left\{ \begin{array}{ll} -7/25t - 13, & y^t_{comp} = 1 \\ 15/67t - 15 \times 92/67 - 5, & y^t_{comp} = 0 \end{array} \right\} \\ \Rightarrow T^{t+1}_f &= T^t_f - \frac{7}{25}\Delta t y^t_{comp} + \frac{15}{67}\Delta t(1 - y^t_{comp}) \end{aligned} \tag{53}$$

for the freezer and $T_r^{t+1} = T_r^t - 3.5/25\Delta t y_{comp}^t + 7.25/67\Delta t(1 - y_{comp}^t)$ for the fridge. Figure 9 presents simulation results for the linearizations. They agree well with the reference model [12]. We thus obtain (42) to (52). The *Fraction of step* idea can be applied by relaxing y_{comp}^t.

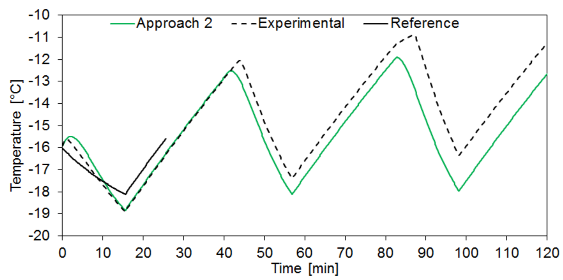

Figure 8: Our results compared to experimental results and reference model from [12] (freezer temperature).

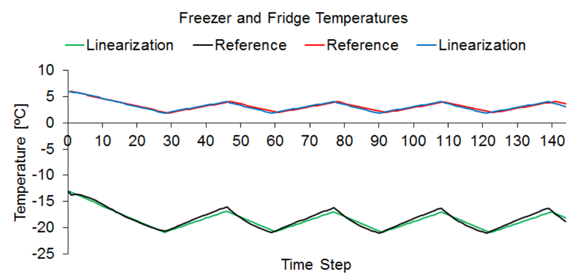

Figure 9: Comparison of simulation results for fridge (freezer) from linearization and reference model.

2.8 Plug-in hybrid Electric Vehicle (EV)

EV is modeled by constraints (54) to (85). Let ϱ^t be the vector $[y_{EVbat}^{dch,t}, y_{EVbat}^{ch,t}, y_{EVfloat}^t]\ \forall\, t \in T$.

$$EVSOC^{t+1} = EVSOC^t + \frac{100\Delta_{t_2}}{EEV_{bat}}\left(P_{EVbat}^{ch,t}\eta_{Ev}^{ch}\mu_{Ev} - \frac{P_{EVbat}^{dch,t}}{\eta_{Ev}^{dch}\mu_{Ev}} - EVp_{loss}y_{EVfloat}^t\right)$$
$$\forall\, t \in T\backslash\{|T|\}, s \in \{1..n_{trips}\} : t_{start}^s \le i < t_{end}^s, t_{start}^1 \le t < t_{end}^1 \quad (54)$$

$$EVSOC^{t+1} = EVSOC^t + \frac{100\Delta t}{EEV_{bat}}\left(P_{EVbat}^{ch,t}\eta_{Ev}^{ch}\mu_{Ev} - \frac{P_{EVbat}^{dch,t}}{\eta_{Ev}^{dch}\mu_{Ev}} - EVp_{loss}y_{EVfloat}^t\right)$$
$$\forall\ s \in \{1..n_{trips}\}, t \in \{1..t_{end}^1 - 1\} \cup \{t_{start}^s..t_{end}^{s+1} - 1\} : t_{start}^1 > t_{end}^1 \quad (55)$$

$$EVSOC^t \ge 0 \qquad \forall\, t \in T \quad (56)$$

$$EVSOC^t \le \begin{matrix} EVSOC_{max}+ \\ (100-EVSOC_{max})y_{EVfloat}^t \end{matrix} \qquad \forall\, t \in T \quad (57)$$

$$EVSOC^1 = EVSOC\_last\_day :\ t_{start}^1 > t_{end}^1 \quad (58)$$

$$EVSOC^{t_{start}^1} = EVSOC_{ret} :\ t_{start}^1 < t_{end}^1 \quad (59)$$

$$EVSOC^{t_{start}^s} = EVSOC^{t_{end}^s} - 100\frac{Km_{next}^s - Km_{fuel}^s}{Km^{100}} \qquad \forall\ s \in \{1..n_{trips}\} : t_{start}^1 > t_{end}^1 \quad (60)$$

$$EVSOC^{t_{start}^{s+1}} = EVSOC^{t_{end}^s} - 100\frac{Km_{next}^s - Km_{fuel}^s}{Km^{100}} \qquad \forall\ s \in \{1..n_{trips} - 1\} : t_{start}^1 < t_{end}^1 \quad (61)$$

$$EVSOC^{t_{end}^s} \ge EVSOC_{min}^{end} \qquad \forall\ s \in \{1..n_{trips}\} \quad (62)$$

$$EVSOC^{t_{end}^{n_{trips}+1}} \ge EVSOC_{min}^{end} : t_{start}^1 > t_{end}^1 \quad (63)$$

$$P_{EVbat}^{ch,t} \le \frac{EVP_{max}^{ch}}{\eta_{Ev}^{ch}\mu_{Ev}} y_{EVbat}^{ch,t} \qquad \forall\, t \in T \quad (64)$$

$$P_{EVbat}^{ch,t} \ge \frac{EVP_{min}^{ch}}{\eta_{Ev}^{ch}\mu_{Ev}} y_{EVbat}^{ch,t} \qquad \forall\, t \in T \quad (65)$$

$$P_{EVbat}^{dch,t} \le EVP_{max}^{dch}\eta_{Ev}^{dch}\mu_{Ev}y_{EVbat}^{dch,t} \qquad \forall\, t \in T \quad (66)$$

$$P_{EVbat}^{dch,t} \ge EVP_{min}^{dch}\eta_{Ev}^{dch}\mu_{Ev}y_{EVbat}^{dch,t} \qquad \forall\, t \in T \quad (67)$$

$$y_{EVbat}^{dch,t} + y_{EVbat}^{ch,t} \le 1 \qquad \forall\, t \in T \quad (68)$$

$$\varrho^t = 0 \qquad \forall\ s{\in}\{1..n_{trips}\}, t{\in}\{t_{end}^s{\le}t{<}t_{start}^s\}:\ t_{start}^1{>}t_{end}^1 \quad (69)$$

$$EVSOC^t = 0 \qquad \forall\ s{\in}\{1..n_{trips}\}, t{\in}\{t_{end}^s{<}t{<}t_{start}^s\}:\ t_{start}^1{>}t_{end}^1 \quad (70)$$

$$\varrho^t = 0 \qquad \forall\, t \in \{t_{end}^{n_{trips}+1}..|T|\}\ \ : t_{start}^1 > t_{end}^1 \quad (71)$$

$$EVSOC^t = 0 \quad \forall\, t \in \{t_{end}^{n_{trips}+1} + 1..|T|\} \ : t_{start}^1 > t_{end}^1 \tag{72}$$

$$\varrho^t, EVSOC^t = 0 \quad \forall\, t \in \{1..t_{start}^1 - 1\} : t_{start}^1 < t_{end}^1 \tag{73}$$

$$\varrho^t = 0 \quad \forall\, s \in \{1..n_{trips}-1\}, t \in \{t_{end}^s..t_{start}^{s+1}-1\} : t_{start}^1 < t_{end}^1 \tag{74}$$

$$EVSOC^t = 0 \quad \forall\, s \in \{1..n_{trips}-1\}, t \in \{t_{end}^s+1..t_{start}^{s+1}-1\} : t_{start}^1 < t_{end}^1 \tag{75}$$

$$\varrho^t = 0 \quad \forall\, t \in \{t_{end}^{n_{trips}}..|T|\} : t_{start}^1 < t_{end}^1 \tag{76}$$

$$EVSOC^t = 0 \quad \forall\, t \in \{t_{end}^{n_{trips}} + 1..|T|\} : t_{start}^1 < t_{end}^1 \tag{77}$$

$$C_{ev}^s \geq Km_{fuel}^s P_{gas} \quad \forall\, s \in \{1..n_{trips}\} \tag{78}$$

$$C_{ev} \geq \sum_{s=1}^{n_{trips}} C_{ev}^s \tag{79}$$

$$y_{EVbat}^{dch,t} \in \{0,1\} \quad \forall\, t \in T \tag{80}$$

$$y_{EVbat}^{ch,t} \in \{0,1\} \quad \forall\, t \in T \tag{81}$$

$$y_{EVfloat}^t \in \{0,1\} \quad \forall\, t \in T \tag{82}$$

$$C_{ev}^s \geq 0 \quad \forall\, s \in \{1..n_{trips}\} \tag{83}$$

$$Km_{fuel}^s \geq 0 \quad \forall\, s \in \{1..n_{trips}\} \tag{84}$$

$$C_{ev} \geq 0 \tag{85}$$

Constraints (54) and (55) establish the relationships between the state of charge, the discharging and charging powers, and the float loss. The vehicle could arrive without energy, so constraints (56) place a lower bound of zero on the SOC. Constraints (57) place an upper bound on the float losses that is activated when a threshold is reached. Constraints (58) and (59) establish an initial value for the SOC. The former is activated when the first event is a departure, and the latter is activated when the first event is an arrival. Constraints (60) and (61) create a link between consecutive trips to ensure energy conservation. Constraints (62) and (63) place a lower bound on the SOC (sufficient to reach the nearest gas station) in intervals when travel is necessary. Constraints (64) to (67) establish bounds on the discharging and charging power. Constraints (68) ensure that at each $t \in T$ the battery either charges or discharges. Constraints (69) to (77) ensure null values for the intervals when the EV battery cannot be used. Constraints (78) calculate the fuel cost for each trip s. Constraint (79) gives the total cost of the fuel consumption. Constraints (80) to (85) are the binary and nonnegative restrictions.

An EV model is essentially the same as a battery model [8], but there are more constraints, including minimal SOC constraints and trip-signal constraints to ensure that the EV charges and discharges only when at home. Sousa et al. [76] present an EV model that is similar to a battery model. Our model is based on [8] and [76] and considers multi-trips in a day [56]. In addition, we consider hybrid vehicles. The *Fraction of step* idea can be applied by relaxing the binaries variables.

2.9 CHP

CHP is modeled by constraints (86) to (110).

$$y_{CHP}^{\tau} \geq z_{CHP}^t \quad \forall\, t \in T, \tau \in \{t..min(t + \lceil \tfrac{d_{CHP}^{on}}{\Delta t} \rceil - 1, |T|)\} \tag{86}$$

$$y_{CHP}^{\tau} \leq 1 - zd_{CHP}^t \quad \forall\, t \in T, \tau \in \{t..min(t + \lceil \tfrac{d_{CHP}^{off}}{\Delta t} \rceil - 1, |T|)\} \tag{87}$$

$$z_{CHP}^{t+1} \leq 1 - y_{CHP}^t \quad \forall\, t \in \{1..|T|-1\} \tag{88}$$

$$zd_{CHP}^{t+1} \leq y_{CHP}^t \quad \forall\, t \in \{1..|T|-1\} \tag{89}$$

$$z_{CHP}^t \geq y_{CHP}^t - y_{CHP}^{t-1} \quad \forall\, t \in \{2..|T|\} \tag{90}$$

$$zd_{CHP}^t \geq -y_{CHP}^t + y_{CHP}^{t-1} \quad \forall\, t \in \{2..|T|\} \tag{91}$$

$$1 \geq zd_{CHP}^t + z_{CHP}^t \quad \forall\, t \in T \tag{92}$$

$$z^1_{CHP} \geq y^1_{CHP} - y^{last\_day}_{CHP} \tag{93}$$
$$y^1_{CHP} = y^{ini}_{CHP} \tag{94}$$
$$P^1_{CHPe} = P^{ini}_{CHPe} \tag{95}$$
$$P^{t+1}_{CHPe} \geq -max(P^{1,\mu}_{CHP,max}, P^{1,\eta}_{CHP,max}) zd^{t+1}_{CHP} + P^t_{CHPe} - 60\Delta t_2 r^{down}_{CHP} w^t_{down} \quad \forall\ t{\in}\{1..|T|-1\} \tag{96}$$
$$P^{t+1}_{CHPe} \leq max(P^{1,\mu}_{CHP,max}, P^{1,\eta}_{CHP,max}) z^{t+1}_{CHP} + P^t_{CHPe} + 60\Delta t_2 r^{up}_{CHP} w^t_{up} \quad \forall\ t{\in}\{1..|T|-1\} \tag{97}$$
$$1 \geq w^t_{up} + z^{t+1}_{CHP} \quad \forall\ t{\in}\{1..|T|-1\} \tag{98}$$
$$1 \geq w^t_{down} + zd^{t+1}_{CHP} \quad \forall\ t{\in}\{1..|T|-1\} \tag{99}$$
$$w^t_{up} \leq y^t_{CHP} \quad \forall\ t \in T \tag{100}$$
$$w^t_{down} \leq y^t_{CHP} \quad \forall\ t \in T \tag{101}$$
$$P^t_{CHPe} \geq max(P^{1,\mu}_{CHP,max}, P^{1,\eta}_{CHP,max}) y^t_{CHP} \quad \forall\ t \in T \tag{102}$$
$$P^t_{CHPe} \leq min(P^{nb^{\mu}_{CHP},\mu}_{CHP,max}, P^{nb^{\eta}_{CHP},\eta}_{CHP,max}) y^t_{CHP} \quad \forall\ t \in T \tag{103}$$
$$P^t_{CHPe} + P^t_{CHPt} = P^t_{CHP,fuel}\bar{\eta} \quad \forall\ t \in T \tag{104}$$
$$P^t_{CHPt} = P^t_{CHPe}\bar{\mu} \quad \forall\ t \in T \tag{105}$$
$$C^t_{CHP} \geq P^t_{CHP,fuel} P_{KW} \Delta_{t_2} \quad \forall\ t \in T \tag{106}$$
$$z^t_{CHP}, zd^t_{CHP} \in \{0,1\} \quad \forall\ t \in T \tag{107}$$
$$y^t_{CHP} \in \{0,1\} \quad \forall\ t \in T \tag{108}$$
$$w^t_{up}, w^t_{down} \leq 1 \quad \forall\ t \in T \tag{109}$$
$$w^t_{up}, w^t_{down} \geq 0 \quad \forall\ t \in T \tag{110}$$

Constraints (86) to (93) control the on/off status of the CHP. Constraints (94) and (95) initialize the status variable and the associated electricity production. Constraints (96) to (101) enforce ramp-up and ramp-down limits. Constraints (102) to (103) place lower and upper bounds on the electricity generated by the CHP. Constraints (104) to (105) relate to the CHP operation. Constraints (106) measure the CHP fuel cost. Constraints (107) to (110) impose the variable domains.

Our model is based on [38] and [39] where efficiency is a function of the electrical power generated. The image of that function has values that are close to each other, so we consider the average efficiency to be a parameter rather than a variable. Variables z^t_{CHP} and zd^t_{CHP} can be relaxed because of Constraints (102) and (103).

2.10 A_{IEUI}: Set of inelastic appliances with uninterruptible operation

Having $\Phi_a = |T| - (\lceil \frac{D_a}{\Delta t_2} \rceil - 1)$, A_{IEUI} is modeled by constraints (111) to (122).

$$x^{t+h}_a \geq P^h_a y^t_a \quad \forall\ a{\in}A^t_{IEUI},\ \forall\ t{\in}T,\ \forall\ h{\in}\{0,\ldots,\lceil \tfrac{D_a}{\Delta t_2} \rceil -1\}:\ t+h \leq |T| \tag{111}$$
$$x^t_a \leq \sum_{i=max(1,t-(\lceil \frac{D_a}{\Delta t_2} \rceil -1)+1)}^{t} P^{t-i}_a y^i_a \quad \forall\ a{\in}A^t_{IEUI},\ \forall\ t{\in}T \tag{112}$$
$$y^t_a = 0 \quad \forall\ a \in A^t_{IEUI}, t \in T : t > \Phi_a \tag{113}$$
$$\sum_{t=1}^{\Phi_a} y^t_a + \zeta_a = 1 \quad \forall\ a \in A^t_{IEUI} \tag{114}$$
$$\sum_{tt=1}^{\Phi_a} tt y^{tt}_a \geq \sum_{t=1}^{\Phi_b} t y^t_b + (\lceil \frac{D_b}{\Delta t_2} \rceil)(1-\zeta_b) - |T| y_{b,a}$$
$$\forall\ a{\in}A^t_{IEUI},\ \forall\ b{\in}A^t_{IEUI}\ \forall\ k{\in}A_{IEUI}{:}a{\in}A^{t,k}_{IEUI}, b{\in}A^{t,k}_{IEUI} \tag{115}$$

$$\sum_{tt=1}^{\Phi_b} tty_b^{tt} \geq \sum_{t=1}^{\Phi_a} ty_a^t + (\lceil \frac{D_a}{\Delta t_2} \rceil)(1-\zeta_a) - |T|(1-y_{b,a})$$

$$\forall\ a\in A_{IEUI}^t,\ \forall\ b\in A_{IEUI}^t\ \forall\ k\in A_{IEUI}: a\in A_{IEUI}^{t,k}, b\in A_{IEUI}^{t,k} \quad (116)$$

$$U_a^t \geq 0 \qquad \forall\ a \in A_{IEUI}^t,\ \forall\ t \in T \quad (117)$$

$$U_a^t \geq S_a y_a^t - ty_a^t \qquad \forall\ a \in A_{IEUI}^t,\ \forall\ t \in T \quad (118)$$

$$U_a^t \geq -DS_a y_a^t + ty_a^t \qquad \forall\ a \in A_{IEUI}^t,\ \forall\ t \in T \quad (119)$$

$$\zeta_a \geq 0 \qquad \forall\ a \in A_{IEUI}^t \quad (120)$$

$$y_a^t \in \{0,1\} \qquad \forall\ a \in A_{IEUI}^t,\ \forall\ t \in T \quad (121)$$

$$y_{b,a} \in \{0,1\} \qquad \forall\ a\in A_{IEUI}^t,\ \forall\ b\in A_{IEUI}^t\ \forall\ k\in A_{IEUI}: a\in A_{IEUI}^{t,k}, b\in A_{IEUI}^{t,k} \quad (122)$$

Constraints (111) and (112) assign the load profile of task $a \in A_{IEUI}^t$ to time $t \in T$. Constraints (113) eliminate solutions where the appliance cannot start its operation. Constraints (114) ensure that the task is done at most once, between the beginning of the horizon and the last start time permitting the completion of the task. Constraints (115) and (116) prevent overlap between tasks for the same appliance. Constraints (117) to (119) count the discomfort from the deviation from the preferred time. Constraints (121) and (122) are the binary restrictions.

A_{IEUI} is a set of inelastic appliances with uninterruptible operation (see [68]). In practice, the operation of these appliances is represented by a load profile. Load profiles forecast the power variation over a period of time for an appliance, frequently as an average. They are a useful approximation. For example, Tsagarakis et al. [80] use aggregated load profiles, while [63] uses load profiles for specific machines. The former use a time-use survey (TUS) to construct the load profiles. However, the consumption found through TUS diaries can be different from the load measurements obtained by submetering [77]. The latter approach uses controlled tests to measure consumption, and the resulting profiles provide a good approximation. UK-DALE [43] is an open-access data-set giving the consumption of domestic appliances in the UK. The data are based on measurements of real electricity consumption.

Our model is task oriented, an idea from [41] that proposes a model with parameters to indicate how many times each appliance will be used. In our case, we consider individual load profiles for each use of each appliance. Therefore, our model includes also appliances that are used intermittently, accordingly with classification in [68].

2.11 A_{phases}

Having $\mho_a^1 = |T| - (\lceil \frac{\sum_{p=1}^{PH_a} D_{a,p}}{\Delta t_2} \rceil - 1)$, $\mho_a^2 = |T| - (\lceil \frac{D_{a,PH_a}}{\Delta t_2} \rceil - 1)$ and $\mho_a^3 = (\lceil \frac{D_{a,PH_a}}{\Delta t_2} \rceil)$, A_{phases} is modeled by constraints (123) to (137).

$$x_a^{t+h} \geq P_{a,p}^h y_{a,p}^t \qquad \begin{array}{c}\forall\ a\in A_{Phases}^t,\ \forall\ t\in T,\\ \forall\ p=1..PH_a\ \forall\ h\in\{0,\ldots,\lceil \frac{D_{a,p}}{\Delta t_2}\rceil - 1\}:\ t+h\leq |T|\end{array} \quad (123)$$

$$x_a^t \leq \sum_{p=1}^{PH_a} \sum_{\substack{i=max(1,t-\\ (\lceil \frac{D_{a,p}}{\Delta t_2}\rceil -1)+1)}}^{t} P_{a,p}^{t-i} y_{a,p}^i \qquad \forall\ a\in A_{Phases}^t,\ \forall\ t\in T \quad (124)$$

$$y_{a,p}^t = 0 \qquad \begin{array}{c}\forall\ a\in A_{Phases}^t,\ \forall\ p=1..PH_a,\\ \forall\ t\in T: t>|T|-(\lceil \frac{D_{a,|PH_a|}}{\Delta t_2}\rceil -1)\end{array} \quad (125)$$

$$\sum_{t=1}^{|T|-(\lceil \frac{D_{a,p}}{\Delta t_2}\rceil -1)} y_{a,p}^t + \Psi_{a,p} = 1 \qquad \forall\ a\in A_{Phases}^t,\ \forall\ p=1\ldots PH_a \quad (126)$$

$$\sum_{tt=t}^{|T|} y_{a,p}^{tt} + \sum_{tt=1}^{t-1+\lceil \frac{D_{a,p}}{\Delta t_2}\rceil} y_{a,p+1}^{tt} \leq 1 \qquad \begin{array}{c}\forall\ a\in A_{Phases}^t,\ \forall\ p=1\ldots PH_a-1\\ \forall\ t\in T\ :\ t\ <\ |T|+1-\lceil \frac{D_{a,p}}{\Delta t_2}\rceil\end{array} \quad (127)$$

$$\sum_{tt=1}^{\mho_a^1} tty_{a,1}^{tt} \geq \sum_{t=1}^{\mho_b^2} ty_{b,PH_b}^t + \mho_b^3(1-\Psi_{b,1}) - |T|y_{b,a}^p$$

$$\forall\ a\in A_{Phases}^t, b\in A_{Phases}^t, k\in A_{Phases}: a\in A_{Phases}^{t,k}, b\in A_{Phases}^{t,k} \quad (128)$$

$$\sum_{tt=1}^{\mho_b^1} tty_{b,1}^{tt} \geq \sum_{t=1}^{\mho_a^2} ty_{a,PH_a}^t + \mho_a^3(1-\Psi_{a,1}) - |T|(1-y_{b,a}^p)$$

$$\forall\ a\in A_{Phases}^t, b\in A_{Phases}^t, k\in A_{Phases}: a\in A_{Phases}^{t,k}, b\in A_{Phases}^{t,k} \quad (129)$$

$$U_a^t \geq 0 \qquad \forall\ a \in A_{Phases}^t,\ \forall\ t \in T \quad (130)$$

$$U_a^t \geq S_a y_{a,1}^t - ty_{a,1}^t \qquad \forall\ a \in A_{Phases}^t,\ \forall\ t \in T \quad (131)$$

$$U_a^t \geq -DS_a y_{a,1}^t + ty_{a,1}^t \qquad \forall\ a \in A_{Phases}^t,\ \forall\ t \in T \quad (132)$$

$$U_a^t \geq F_a y_{a,PH_a}^t - ty_{a,PH_a}^t \qquad \forall\ a \in A_{Phases}^t,\ \forall\ t \in T \quad (133)$$

$$U_a^t \geq -DF_a y_{a,PH_a}^t + ty_{a,PH_a}^t \qquad \forall\ a \in A_{Phases}^t, t \in T \quad (134)$$

$$\Psi_{a,p} \geq 0 \qquad \forall\ a \in A_{Phases}^t,\ \forall\ p = 1..PH_a \quad (135)$$

$$y_{a,p}^t \in \{0,1\} \qquad \forall\ a \in A_{Phases}^t,\ \forall\ t \in T,\ \forall\ p = 1..PH_a \quad (136)$$

$$y_{b,a}^p \in \{0,1\} \qquad \begin{array}{c}\forall\ a\in A_{Phases}^t,\ \forall\ b\in A_{Phases}^t \\ \forall\ k\in A_{Phases}: a\in A_{Phases}^{t,k}, b\in A_{Phases}^{t,k}\end{array} \quad (137)$$

Constraints (123) and (124) assign the load profile of each phase p of task $a \in A_{phases}^t$ to time $t \in T$. Constraints (125) eliminate solutions where the appliance cannot start its operation. Constraints (126) ensure that the task is done at most once, between the beginning of the horizon and the last start time permitting the completion of the task. Constraints (127), from [20], are precedence constraints between consecutive phases of the same task. Constraints (128) and (129) prevent overlap between tasks for the same appliance. Constraints (130) to (134) count the discomfort from the deviation from the preferred time. Constraints (136) and (137) are the binary restrictions.

Each load profile is separated in sequential phases, and the operation can be interrupted between phases. The appliances in A_{phases} include dishwashers [10], washing machines [66], and dryers [63].

The model has flexibility enough to accommodate other constraints if the client need it. For example, if there is a need of maximum time Max^t, between phases, we can add $\forall\ a \in A_{Phases}^t, p = 1...PH_a - 1$:

$$\sum_{tt=1}^{|T|} tty_{a,p+1}^{tt} - \sum_{t=1}^{|T|} ty_{a,p}^t \leq Max^t.$$

If, for instance, the dryer d are going to be used after the washing machine b, we can add:

$$\sum_{tt=1}^{|T|-LL} tty_{d,1}^{tt} \geq \sum_{t=1}^{|T|-(\lceil \frac{D_{b,PH_b}}{\Delta t_2} \rceil - 1)} \left(t + \left\lceil \frac{D_{b,PH_b}}{\Delta t_2} \right\rceil\right) y_{b,PH_b}^t \text{ where } LL = \left\lceil \sum_{p=1}^{PH_d} D_{d,p} \frac{1}{\Delta t_2} \right\rceil - 1.$$

2.12 Other constraints

IBR constraints:

$$E_g^{t,i} \leq E_{th}^t \qquad \forall\ t \in T, i \in B \quad (138)$$

$$\Delta_t \sum_{t\in T} E_g^{t,i} \leq E\_bl^i \qquad \forall\ i \in B \quad (139)$$

$$\Delta_t E_g^{t,i} \leq E\_bl^i y_g^i \qquad \forall\ t \in T, i \in B \quad (140)$$

$$\sum_{i\in B} y_g^i \leq 1 \quad (141)$$

$$y_g^i \in \{0,1\} \qquad \forall\ i \in B \quad (142)$$

Constraint (138) limits the energy that can be bought. Constraints (139) to (142) are the main IBR constraints. (139) ensures that the daily consumption is within the capacity. (140) controls the activation of the blocks, and (141) ensures that at most one block is used. (142) are the binary restrictions.

Flow conservation :

$$\sum_{a\in A} x_a^t = 10^3(p_{EVbatt}^{ch,t} + P_{bat}^{ch,t} - P_{bat}^{dch,t} - p_{EVbatt}^{dch,t} - P_{CHPe}^t) + E_{pv}^t - E_v^t + E_{wt}^t + \sum_{i\in B} E_g^{t,i} \quad \forall\, t \in T \tag{143}$$

The coupling constraints (143) ensure energy conservation.

Financial incentives :

$$C^t = \Delta_t \left[\lambda^t \left(\sum_{i\in B}(1-\varpi^i)E_g^{t,i}\right) - \nu^t E_v^t\right] \quad \forall\, t \in T \tag{144}$$

$$E_v^t \leq E_{th}^t \quad \forall\, t \in T \tag{145}$$

Constraints 144 represent the cost at each time t is given by the energy acquisition cost for block i minus the energy sold plus the price of CHP. Inequality (145) limits the energy that can be sold. Variable E_v^t represents the case where the customer can inject electricity into the grid. In some markets, the customer receives in exchange an energy credit for future consumption. In this case, we set $E_v^t = 0$ in (144), rewrite (143) as (147), and replace constraint (145) by $E_{av}^0 = 0$ to initialize the power credit variable.

Objective function :

$$\min_{\Xi}\; w_c\left(\sum_{t\in T} C^t + C_{ev} + C_{CHP}^t\right) + w_t \sum_{t\in T}\sum_{a\in A} V_a^t + w_u\left[\sum_{a\in A_{phases}^t}\sum_{p=1}^{|PH_a|}\Psi_{a,p} + \sum_{a\in A_{IEUI}^t}\zeta_a + \sum_{t\in T}\sum_{a\in A^t} U_a^t\right] \tag{146}$$

We minimize a weighted sum of comfort and cost (146), where the cost is given by (144) and the EV cost.

3 Data and instances

In this section we discuss our data and how we create the instances.

3.1 Locations

Brazil is expected to become one of the largest smart-grid markets in the world by 2023 [34]. The country has a total installed capacity of 161 GW [6], which is expected to grow to 224 GW by 2030 [31, Table 6.26] via initiatives such as the Cities of the Future Project [16]. An analysis of the smart grid development in Brazil is performed in [27]. The climatic data was taken from [4, Chapter 14]. We calculated the temperature based on 5% dry-bulb design conditions. Wind speed data was taken from [47].

3.2 Prices

In Brazil, there are two pricing options: the conventional tariff and the white tariff. The conventional tariff is constant, whereas the white tariff is a TOU pricing with a single price for weekends and holidays and three weekday prices:

1. Peak hours: Three consecutive daily hours defined by the distributor.
2. Intermediate peak hours: The hour before and the hour after the peak hours.
3. Nonpeak hours: The remaining hours of the day.

We use the electricity prices published in April 2017 for the white tariff. We summed two tariffs, following [50, p. 57].

The IBR pricing defined by federal law [14] specifies certain discounts:

1. For the portion of consumption below 30 kWh/month, the discount is 65%.
2. For the portion between 31 and 100 kWh/month, the discount is 40%.
3. For the portion between 101 and 220 kWh/month, the discount is 10%.

We divided the monthly limits defined above by 30 days. This makes our model less realistic compared to the actual reality, but since smart meters track and report energy consumption in intervals of minutes, we suppose that a pricing scheme in the day will be more important than in the whole month. The law applies to a subgroup of the population, but we apply it to everyone.

Brazil has a net metering incentive. If the energy injected into the grid is greater than that consumed, the customer receives an energy credit for future consumption. In addition, we assume that, as in other markets, Brazil's consumers will in the future have the opportunity to sell electricity, i.e., a *feed-in tariff*. Thus, we consider $\nu^t = \frac{\lambda^t}{2}\ \forall\ t \in T$.

3.3 Capacity

We set the capacity E^t_{th} to 75 kW, which is the residential capacity in Brazil.

3.4 PV and solar collector

We take the data from data-sheets or use the estimates in [29]. We consider the PVs *Canadian Solar CS5P250M*, *Yingli Solar JS150*, and *Siemens SM110* and the solar collectors *CSi Sodramar*, *TERMOMAX*, *Soletrol*, and *Sunda Seido 10*. The ground reflectance was generated from the uniform distribution U(0.13,3) according to [4, Table 5, Chapter 14].

3.5 Wind turbines

The data comes from the data-sheets for the *Raum Energy 3.5 kW Wind Turbine System* and the *Raum Energy 1.3 kW Wind Turbine System*.

3.6 HVAC

For the house, we generated resistance values from a uniform distribution (see [72]), converting the units to (m^2 ^{o}C.h/J). The house height is 3.048 m, with $A_{ceiling} = A_{floor} = 100$ m^2. We set $P_{heating} = P_{cool} = 60\frac{W}{m^2} \times A_{floor}$, an approximate value suggested by some manufacturers. We set A_{ul} between 0.7 and 2.8. We set IDF to 0.031 for cooling and 0.086 for heating. The other parameters are $T^t_f = 23^oC\ \forall\ t \in T$, $H^t_p = 97.57W\ \forall\ t \in T$.

3.7 Water heaters and shower

We use $T^{chu}_f = T^{wh}_f = 50^oC$ (see [48]). We set $P_{wh} \sim U(4000, 5000)W$ (see [72]). The heat resistance is given by $U(12, 25)\frac{^oFft^2h}{Btu}$ converted to (m^2 ^{o}C.h/J). We take the WH area and diameter from the data-sheets for Giant-142ETE, Giant-152ETE, Giant-172ETE, Rheem-PROPH50, Rheem-PROPH65, and Rheem-PROPH80. We use the diameter to calculate $(UA)_{wh}$ and V_{tank}. We set $T^{max} = 100^oC$ and $E_{wh} = 1$.

We took the temperature of the water from the street (T^t_{inlet}) from [22, Graphic 4]. We projected the missing intervals so that the last projected value is equal to the first collected value.

For fr^t_{wh} and fr^t_{chu}, we used the data available in [26]. For each client, we aggregate the daily consumption in intervals of Δ_t. Inter-period consumption is calculated proportionally. P_{chu} is obtained from the data-sheets for Lorenzetti's showers.

3.8 Batteries

We used the following values from [88]: $E_{bat} = 24\,\text{kWh}$, $SOC_{min} = 20\%$, $SOC_{max} = 100\%$, $p^{ch}_{max} = 4\,\text{kW}$, $p^{dch}_{max} = 4\,\text{kW}$, $p^{ch}_{min} = 0.3\,\text{kW}$, $p^{dch}_{min} = 0.3\,\text{kW}$, $\eta^{ch} = 0.91$, $\eta^{dch} = 0.91$, $\mu = 1$. According to [15], in a low-storage system, the float charge losses represent around 100 W, so $p_{loss} = 0.1\,\text{kW}$.

3.9 Fridge

The fridge is described in [13] and [12]. The other parameters are $T^{start}_{freezer} = -13^o\text{C}$, $T^{start}_{refri} = 6^o\text{C}$, $P_{comp} \sim U(150, 170)\,\text{W}$ considering permanent regime from [21], $T^{freezer}_{f} = -18^o\text{C}$, and $T^{refri}_{f} = 2^o\text{C}$.

3.10 Electric vehicles

We used the Nissan Leaf's battery specifications [59]: $EV_{bat} = 24\,\text{kWh}$, $EVSOC_{max} = 90\%$, $EVSOC_{min} = 0\%$ and $EVP^{ch}_{max} = EVP^{dch}_{max} = 3.6\,\text{kW}$. The other parameters are based on the battery parameters: $EVP^{ch}_{min} = EVP^{dch}_{min} = 0.3\,\text{kW}$, $EV\mu = 1$, and $EVp_{loss} = 0.1\,\text{kW}$.

The Nissan Leaf has a battery capacity of 24 kWh and a range of 160 km [76]. We calculated $km^{100} = \frac{EV_{bat}}{Electricity\ consumption} = \frac{24\,kWh}{150\,Wh/km} = 160\,\text{km}$, as in [76].

We simulated the battery-charging model for 7 h. At time 0, the SOC was 0. With the specified rate of 3.6 kW/h, the SOC should be 25.2 kWh after 7 h. We therefore defined $\eta^{dch}_{ev} = 24/25.2 \approx 0.95$. Moreover, we set $\eta^{dch}_{ev} = \eta^{ch}_{ev}$.

The number of trips is set to $n_{trip} \sim U(1, 4)$ and t^s_{start} and t^s_{end} are generated randomly. The first trip has a minimum duration of 8 h, the second 4 h, the third 1 h, and the fourth 0.5 h.

The other parameters are $price\_gas = 3\,\$/\text{l}$, $cons\_gas = 10\,\text{km/l}$, $EVSOC\_last\_day = 50\%$, $Km^s_{next} \sim U(0, km^{100})\,km\ \forall\ s \in \{1, ..., n_{trip}\}$, $EVSOC^{end}_{min} \sim U(EVSOC_{ret}, \text{MM})\%$, where MM = maximum value of $EVSOC_{ret}$, and finally, $EVSOC_{ret} \sim U(0, 30)\%$.

3.11 CHP

We take the data from [39, Table 4] and the data-sheet for CHP CP5WN-SPB. For that CHP, $rate^{fuel}_{CHP} = \frac{0.72\,gallon/h}{17.8\,kWh} = \frac{3.79\,l/gallon \times 0.72\,gallon/h}{17.8\,KWh} = 0.153\,l/kWh$.

Thus, the values are: $d^{on}_{CHP} = d^{off}_{CHP} = 60\,\text{min}$, $nb^{\mu}_{CHP} = nb^{\eta}_{CHP} = 3$, $r^{down}_{CHP} = r^{up}_{CHP} = 0.05\,\text{kW/min}$, $y^{last\_day}_{CHP} = y^{ini}_{CHP} = 0$, and $P^{ini}_{CHPe} = 0\,\text{kW}$. Fixing μ and $\eta \in \{1, 2, 3\}$ we set: $P^{k,\mu}_{CHP,min}$ and $P^{k,\eta}_{CHP,min} \in \{0, 0.2, 0.5\}\,\text{kW}$, $P^{k,\mu}_{CHP,max}$ and $P^{k,\eta}_{CHP,max} \in \{0.2, 0.5, 1\}\,\text{kW}$, $\eta^k_{CHP,p} \in \{0, 80, 85\}$, and $\mu^k_{CHP,p} \in \{0, 40, 35\}$.

We set the overall efficiency to the average of the efficiencies given by the piecewise linear function, discarding null efficiencies. Thus, $\bar{\eta} = 0.825$ and $\bar{\mu} = 0.375$.

3.12 A_{IEUI} and A_{phases}

We use the data from [43]. We start the analysis from the first day that has measured data at midnight. Missing data is assumed to indicate no consumption. We aggregated the power data into 10-min intervals based on the average values. We calculated probabilities for the time and duration of the use of each appliance. Using these probabilities, we selected a time t when that appliance can be started for S_a and its duration D_a. We obtain P^h_a from the aggregated power in the interval between t and $t + D_a$. Finally, we set $DS_a = D_a + U(0, 4)$.

For A_{phases}, we performed the steps above for each phase. Dishwashers have three phases: washing, draining, and drying [10]. We tried to find patterns to break the load profile into these phases: see Figure 10. Washing machines have three phases: water heating, washing, and spinning [66]. Dryers have two phases: with and without heat [63]. In [63], the duration of the dryer's second phase is between 5 and 15 min, so we consider the final 10 min of the load profile to be the second phase.

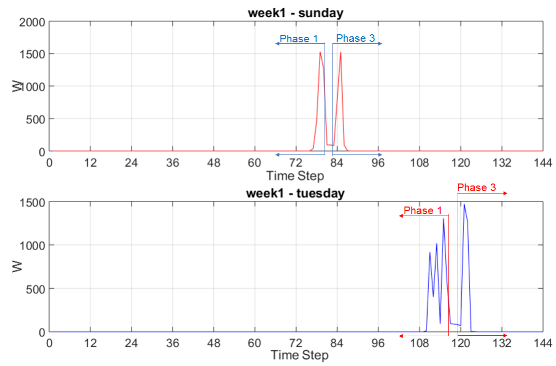

Figure 10: Defining phases in the dishwasher.

4 Results and discussion

In this section, we solve the scheduling problem using various models. We selected the papers from Table 1 that have at least 7 submodels. To perform a fair comparison, we replaced the comfort constraints in every model by a fixed start time for the appliances based on load profiles, and fixed bounds for desired temperatures for the thermal appliances. Thus, comfort is equivalently for every model and the objective function considers only the cost instead of the trade-off between cost and comfort. The parameters not previously defined are as follows: $H = 24$, $|T| = 2$, and $w_c = w_u = w_t = 1$.

4.1 Models from [73]

We consider the appliance models in [74, 73] with the following adjustments:

1. We assume that $S_t^{ESS} = S_t^{ess}$.
2. The available data corresponds to time windows and power for four appliances in [73, Table 1] and electricity prices in [73, Figure 3]. Since the devices based on load profiles have a fixed usage initialization, we use the data from Section 3 instead of that from [73].
3. For the freezer and fridge, the computation of β^{fr}, α^{fr} and γ^{fr} is not specified. We assumed that β^{fr} is related to the action of opening and closing the fridge doors, α^{fr} is related to the evaporator temperature, and γ^{fr} is related to the losses.
4. For HVAC, α^{ac} and α^{ht} are undefined. We assumed that $EP_t = EP_t^{\Theta}\ : \Theta \in \{\text{ac}, \text{ht}\}$. The parameters β^{ac}, β^{ht}, ρ^{ac}, and ρ^{ht} are computed as in our model, considering infiltration and losses based on the structure of the house.
5. For lighting, there is no constraint that associates illumination level with consumption. Therefore, we did not consider this.

We start our experiments with an "initial" combination composed by A_{IEUI}, fridges, WTs, PVs, IBR constraints, and selling options. We progressively add more appliances. Each Instance (Ins.) consists of a combination of appliances. For example, in Table 2, Ins. 2 includes the appliances considered in Ins. 1 plus an ESS.

Table 2: Costs for model from [73] and our model.

Ins.	Combination	[73] cost ($)	Our cost ($)
1	"initial"	4.02	4.02
2	Ins. 1 + ESS	1.61	1.49
3	Ins. 2 + HVAC	1.93	6.83
4	Ins. 3 + CHP, WH	1.93	6.83
5	Ins. 4 + A_{phases}, Shower	-	9.06
6	Ins. 5 + EV	-	30.03
7	Ins. 4 + Boiler, TSS	1.93	-

In Ins. 1, we assign consumption profiles over the horizon and respect the bounds on the freezer and fridge temperatures. Both models give the same cost.

In Ins. 2, we add a battery, a type of ESS. The charging and discharging efficiencies are set to 100%. The model of [73] allows the battery to be off during the entire horizon, but with charging and discharging. Their cost is 8% higher than ours. There are two reasons for this. First, our model considers the SOC at the beginning of an interval, whereas [73] considers it at the end. Thus, in the final interval our model records a discharge while the model from [73] does not. Second, we have lower bounds on the charge and discharge variables. If we remove these two differences, we find the same solution.

In Ins. 3, for the model of [73], HVAC adds 32 cents to the bill while our model adds around 440 cents. Like the ESS, the HVAC is off throughout the horizon, but it contributes to the indoor temperature. As we will see in Ins. 9, the main issue in this experiment is the solar gain.

In Ins. 4, both models adjust the use of fridge and batteries, achieving the same cost as in Ins. 3.

In Ins. 5, 6, and 7, we add appliances that are considered either by our model or by [73], obtaining results for just one of the models.

In Ins. 3, the HVAC and the battery cannot emit or absorb energy if they are not turned on. For example, a battery could have the constraint set $AC_b = \{\text{BatPower}_t \leq \text{BatCapacity} \times y_t^{\text{on,off}} \forall\, t \in T\}$, where $y_t^{\text{on,off}}$ is binary, and similar steps give the constraint set AC_h for HVAC. Table 3 shows the results when we add the sets AC_b and AC_h.

Table 3: Costs for model from [73] and our model, with additional constraints from [73].

Ins.	Combination	[73] cost ($)	Our cost ($)
1	"initial"	4.02	4.02
8	Ins. 1 + ESS, AC_b	2.13	1.49
9	Ins. 8 + HVAC	2.13	6.83
10	Ins. 9 + AC_h	infeasible	6.83
11	Ins. 8 + solar gain	infeasible	6.83
12	Ins. 10 + disjoint set	2.28	6.83
13	Ins. 12 + solar gain	7.34	6.83

For Ins. 8, we note that the model from [73] has a cost around 43% higher than ours. The cost for [73], compared with Ins. 2, is increased because of the battery losses. For Ins. 9, HVAC works without consumption because the activation constraints are not considered. When we add these constraints in Ins. 10, [73] becomes infeasible. Moreover, in Ins. 9, our model consumes energy trying to keep the indoor temperature within the bounds. This does not happen in [73], as shown in Figure 11. The model from [73] does not consider solar gain. This has a considerable effect on the indoor temperature [7], so our model consumes more energy and is more expensive.

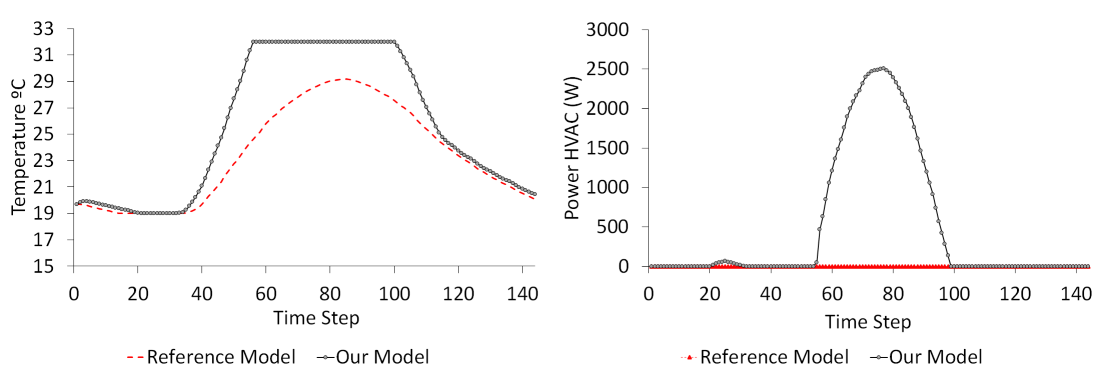

Figure 11: Results for temperature of Ins. 9.

When we add solar gain in Ins. 11, [73] becomes infeasible. Ins. 12 assumes that the time windows (TWs) for the A/C and heating form a disjoint set. The model from [73] now gives a feasible solution. However, there is still no consideration of solar gain, and finding the optimal disjoint set of TWs is difficult since there are $2^{|T|}$ possible combinations. If we remove the solar gain from the analysis, our model decreases the cost by around 280%. Ins. 13 adds solar gain to Ins.12 with only A/C for the disjoint set of TWs for the HVAC to avoid infeasibility. The model from [73] becomes, monetarily, more expensive than ours.

The thermal energy storage model in [73] follows the ESS model, so a similar analysis can be performed. The CHP in [73] comes from [45], and we present this analysis in Section 4.3. Although the original model from [73] gives a lower cost than our model, as for by Ins. 4, our model consider more details, and is closer to reality. The difference between the results of our model and the ones from [73] is ≈ 1715\$ (544USD), which should be planned as expenses.

4.2 Results from [7, 8]

The models from [7, 8] consider equivalent batteries, water heating, and underfloor HVAC models. Moreover, they have the same energy flow conservation constraints.

We discussed the limitations of the battery models in Section 2.6. The water heating model from [7, 8] is given below:

$T_{st}(t+1) = T_{st}(t) + \frac{V_D^{th}(t)}{(V_{tot})}(T_{cw} - T_{st}(t)) + \frac{P_{aux}^{th}(t)+P_{CHP}^{th}(t)}{V_{tot}C_w} - \frac{A_{st}}{R_{st}}(T_{st}(t) - T_b(t)) \ \forall\ t \in T/\{|T|\}$, where V_{tot} is the total WH volume; $V_D^{th}(t)$ is the hourly hot water demand at time t; $T_{cw}(t)$, $T_b(t)$, and $T_{st}(t)$ are the entering cold water, environment around the WH, and hot water temperatures at time t, respectively; A_{st} is the surface area of the WH; and R_{st} is the thermal resistance of the WH insulation material. We need to change the units given in [8]. Using our parameter Δ_{t_2}, we have:

$$T_{st}(t+1) = \frac{V_D^{th}(t)}{(V_{tot})}(T_{cw} - T_{st}(t)) + \Delta_{t_2}\frac{P_{aux}^{th}(t) + P_{CHP}^{th}(t)}{V_{tot}C_w} - \frac{\Delta_{t_2}}{V_{tot}C_w}\frac{A_{st}}{R_{st}}(T_{st}(t) - T_b(t)) + T_{st}(t) \ \forall\ t \in T/\{|T|\}.$$

This modified model is close to our model. There are two differences. First, we use demand as the rate volume per time, but multiplying it by the time interval results in V_D^{th}. The second difference is related to the technology. We use an electrical resistance as the auxiliary power while [7, 8] use a boiler fed by gas. Since gas and electricity have different prices, for a fair comparison, we assume that the three hot water models ([8], [7], and ours) use electricity as auxiliary power. Note that the three models link the HVAC and CHP systems.

Our HVAC is directly in contact with the air that heats the principal floor, while the HVACs from [7, 8] are on the basement floor. Otherwise, the models are equivalent. For a fair comparison, we assume that all the models have the HVAC on the main floor.

The CHP model in [8] differs from that in [7] by a binary on/off variable and one constraint. We test both versions. The *schedulable tasks and residential load* model has more constraints in [8] than in [7], but as we set the starting time for the appliances based on the load profiles, the models are feasible.

Finally, since [7] considers WTs and PVs, we add these to [8]. Thus, the conservation constraints for both come from [7, Equation 37] with $\delta = 1$.

We start our experiments with an "initial" combination composed by the A_{IEUI} and A_{phases} appliances, WTs, PVs, IBR constraints, and selling options. We progressively add more appliances; see Table 4.

In Ins. 1, we assign consumption profiles over the horizon. All the models give the same cost.

In Ins. 2, we add a battery. The charging and discharging efficiencies are set to 100%. For [7, 8] we do not place an upper bound on the initial SOC. Their SOC starts at the maximal value allowed, which gives a result 296% cheaper than our model.

Table 4: Costs for models from [7, 8] and our model.

Ins.	Combination	[8] cost ($)	[7] cost ($)	Our cost ($)
1	"initial"	3.9506	3.9506	3.9506
2	Ins. 1 + ESS	-5.2055	-5.2055	1.3134
3	Ins. 2 + SOC_{min}	1.3102	1.3102	1.3134
4	Ins. 3 + D_A	1.2716	1.2716	2.0013
5	Ins. 1 + HVAC	8.7767	8.7767	8.7767
6	Ins. 3 + HVAC	6.6601	6.6601	6.6629
7	Ins. 6 + D_A	6.5999	6.5999	7.3859
8	Ins. 5 + WH, $\text{CHP}^{\text{off}}_{\text{ini}}$	16.6304	infeasible	9.7961
9	Ins. 5 + WH, $\text{CHP}^{\text{on}}_{\text{ini}}$	infeasible	infeasible	10.5269
10	Ins. 9 + D_A	infeasible	infeasible	-4.4723
11	Ins. 8 + D_A	16.6304	infeasible	-2.4028

Suppose SOC_{min} is the bound on the initial SOC. We add SOC_{min} to the models from [7, 8] in Ins. 3. Then, their results are 0.24% cheaper than our result because they do not specify a minimal power for the charging and discharging variables. If we also add these constraints, we obtain the same cost as for our model.

In Ins. 4, we change the efficiencies to the values in [8]. D_A refers to the data from [8]. Their cost is 36.5% lower than our cost. The most important part of this difference is explained by the energy construction in the battery constraints linked with the energy conservation flow in [7, 8](see Section 2.6).

In Ins. 5 and 6, we test HVAC and HVAC with ESS, respectively. The efficiencies in the battery model are 100%. The results are identical for Ins. 5, and they are slightly different for Ins. 6 for the same reason as in Ins. 3. However, for Ins. 7, with D_A, the [7, 8] results are 10.6% cheaper than ours because of the energy creation.

In Ins. 8, we test the CHP with the WH and HVAC. The CHP is off in the first interval, indicated by $\text{CHP}^{\text{off}}_{\text{ini}}$ in Table 4. In the [8] results, CHP and the boiler were not used. The only way to increase the water temperature is by increasing the room temperature, but this solution is 69.8% more expensive than our results. In [7] the ramp-up constraints do not allow the start-up of the CHP. Moreover, the off status is not allowed. Therefore, the [7] model is infeasible.

In Ins. 9, we changed the CHP status at the first interval. It is on with a maximal production of electrical power, indicated by $\text{CHP}^{\text{on}}_{\text{ini}}$ in Table 4. Constraint 17 from the [8] model makes the problem infeasible, and the upper bound on P^t_{CHPt} in the [7] model makes the problem infeasible.

Ins. 10 and 11 are identical to Ins. 8 and 9, but with D_A. The analysis for Ins. 8 and 9 applies. For Ins. 11, our model sells electricity while the [8] model buys it. Our solution is around 114% (19.03R$) less expensive than the [8] solution. This represents an annual cost of ≈ 6947$ (2205 USD).

4.3 Results from [45]

There are two models from [45] that we did not consider in the analysis: the fridge model (29–31 in [45]) and the HVAC model (32–33 in [45]). These models have a scheduled consumption solution as input. For each interval, the models postpone or advance the time when the appliance will be turned on in that input solution. Thus, [45] assumes that the cooling goods (food), for the fridge, and the living space (air), for the HVAC, have enough thermal inertia to act as a buffer. We do not know how to determine the initial buffers, needed as parameters. We assume we have a scheduled solution for the fridge and a null initial buffer for the cooling goods. We consider only a fridge, and we optimize the electricity cost using the models from [45] and our model. The solution found by [45], shown in Figure 12, is not feasible because the temperatures become too high.

We started our experiments with an "initial" combination composed by the A_{IEUI} and PV appliances, IBR constraints, and selling options. WTs are considered in all the instances except 1, 2, 3, and 6. We progressively add more appliances; see Table 5.

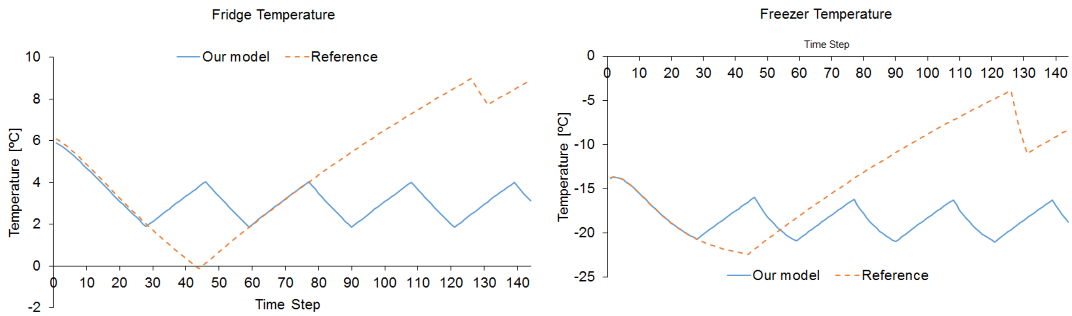

Figure 12: Results for temperature of reference fridge model from [45] and our model.

Table 5: Costs for model from [45] and our model.

Ins.	Combination	[45] cost ($)	our cost ($)
1	"initial"	12.6557	12.6557
2	Ins. 1 + ESS	11.6846	10.4669
3	Ins. 2 + ESS*	11.6463	10.4669
4	Ins. 1 + CHP	12.6557	12.3806
5	Ins. 1 + WT	3.5393	3.5393
6	Ins. 5 + ESS	4.5219	0.8055
7	Ins. 6 + ESS*	4.5219	0.8055
8	Ins. 6 + EV	infeasible	21.8308
9	Ins. 8 + CHP	infeasible	21.8308
10	Every appliance	infeasible	30.0261
11	Ins. 5 + CHP	3.5393	3.521
12	Ins. 11 + off grid, WS	infeasible	20.7146
13	Ins. 5 + EV	infeasible	23.3725
14	Ins. 5 + EV	infeasible	3.9683
15	Ins. 5 + EV*	11.0408	3.9683
16	Ins. 15 + ESS	10.6995	2.7601
17	Ins. 16 + CHP	10.6995	2.7601

In Ins. 1, we assign consumption profiles in the horizon and we consider the production from the PV. Both models give the same cost.

In Ins. 2, we add the ESS. In contrast to [73], the ESS model in [45] is designed specifically for a flywheel. The [45] solution continuously charges and discharges at the same time to maintain feasibility. It is 1.12 times more expensive than our solution.

Given the continuous charging and discharging operation of Ins. 2, in Ins. 3 we assume that the ESS power variables in [45] ($p_{min}^{ess,r}$ and $p_{max}^{ess,r} : r \in \{eex, eim\}$) should be allowed to be zero, allowing the model to either charge or discharge. We change Constraints 10 from [45] to: $y_t p_{min}^{ess,r} \leq p_t^{ess,r} \leq y_t p_{max}^{ess,r}$ $\forall\, r \in \{eex, eim\}, t \in T$, where $y_t \in \{0, 1\}$ is an on/off variable at time t. This is represented by ESS* in Table 5. In the [45] results, the battery does not always charge and discharge at the same time. This explains the cost decrease compared to Ins. 2.

Ins. 4 uses the appliances from Ins. 1 plus CHP. The CHP is off in the first interval. The costs for the two models are almost the same. In our model CHP is used between intervals 99 and 123, and in the [45] model CHP is not used. This will be discussed in our analysis of Ins. 11.

In Ins. 5, we add the production from WT. There is no WT in [45], but it could decrease the cost by a factor of 4 compared with the cost for Ins. 1. We therefore considered WT for the next experiments.

In Ins. 6, we add ESS to Ins. 5. The [45] solution continuously charges and discharges at the same time to maintain feasibility: it is 5.6 times more expensive than our solution. The difference between the [45] solution and our solution is larger in Ins. 6 than in Ins. 2. Moreover, we can compare the cost reduction after the addition of WT, using the results from Ins. 2 and 6. We reduced the cost by a factor of 13 while the [45] model reduced it by 2.6. This is because when there is energy coming from WT, the battery has to be used more to sell energy at high prices. If the battery model has limitations, increased use of the battery will have an impact on the cost. If batteries are not considered, the differences are reduced, as shown by the solutions for Ins. 4 and 11.

We use ESS* for Ins. 7, as in Ins. 3. Compared to Ins. 6, the results do not change because $y_t = 1 \; \forall \; t \in T$. In Ins. 8, 9, and 10, the addition of EVs makes the models from [45] infeasible. We will explain this below.

Ins. 11 has the same appliances as Ins. 5 plus CHP. The CHP is off in the first interval. Our model and the [45] model give similar costs. In our model CHP is used between intervals 113 and 118; in the [45] model it is not used. This is because the ramp-up and ramp-down constraints in [45] do not allow the CHP to change state. This can be problematic when there is more demand or in off-grid systems.

In Ins. 12, we force the use of CHP via an off-grid system. If a surplus of energy occurs, it is lost, i.e., we waste the surplus (WS). Since fuel is more expensive than electricity in our data, the cost of meeting the demand is higher, and it cannot be met by the [45] model because of the ramp-up and ramp-down constraints.

In Ins. 13, we consider the appliances from Ins. 5 plus EV. The infeasibility in the [45] model is because that model cannot consider the case where the vehicle departs at time k_0, returns at time k_1, and departs again at time k_2 ($k_2 > k_1 > k_0$). This implies noncyclic behavior since there is an odd number of departure-arrival events. The bounds $E_t^{evh,ub}$ and $E_t^{evh,lb}$ in the [45] model cannot handle this case.

In Ins. 14, we change the EV parameters to allow only one departure, where the vehicle is plugged in at interval 7 and the departure is at interval 110. Here, the scenario is appropriate for the [45] model, but there is no zero energy assignment when the EV is traveling because of Constraint 22 from [45]. In Ins. 15, we changed this constraint to:

$$e_t^{evh} = e_{t-1}^{evh} + (p_t^{evh,eex}\eta^{evh,eex} - \frac{p_t^{evh,eim}}{\eta^{evh,eim}})\Delta_{t_2} + k_t^{evh}(E_t^{evh,ub} - e_{t-1}^{evh}) \; \forall \; t \in T.$$

This change is indicated by EV* in Table 5. It corrects the problem of Ins. 14, but the inequalities 21 from [45] do not allow the power variables to be zero. This increases the cost, and our cost is around 278% cheaper.

Ins. 16 adds ESS to Ins. 15; Ins. 17 adds CHP to Ins. 16. For both models, ESS reduces the final cost, but CHP does not (it is not used). Our cost is 389% (7.93R$) cheaper. This represents an annual cost of $\approx$ 2894$ (918 USD).

4.4 Application: Day-to-day scheduling

We now present an application of our model to a house in Belo Horizonte, Brazil, during the summer. We used a PC with a 19 Ghz Intel Core i5-4300U and 8 GB of RAM. Figures 13 and 14 show the forecast data, the electricity price, and the behavior of the appliances in the optimal solution.

In the Water Temperature and Water Temperature in Shower plots, a Temp. wish value of zero means that the user does not care about the temperature. The plots show that the temperature needs are almost met. For instance, the water temperature is acceptable for the shower and for general use after step 36. The temperature before step 12 is unacceptable because the WH power and the thermal energy provided by CHP cannot sufficiently increase the initial temperature in the interval before the first and second uses. This is confirmed by the plot *Fraction of time with power on*, which shows that WH is on from the start until near step 12. The CHP operates at a maximal speed until step 12. The air temperature deviates from the target around 12 a.m. because the A/C power is insufficient. Note that in *Fraction of time with power on* the A/C is on whenever the temperature is above the target. The fridge and freezer quickly adjust their internal temperatures.

Discharge mode is preferred for the batteries when the price is high. The customer does not buy energy between steps 96 and 125 because it is too expensive. Moreover, CHP is preferred around those times. The EV makes its planned trips and is used for storage when electricity is expensive, e.g., in the steps around 100. The appliances with load profiles are used during the permitted time windows.

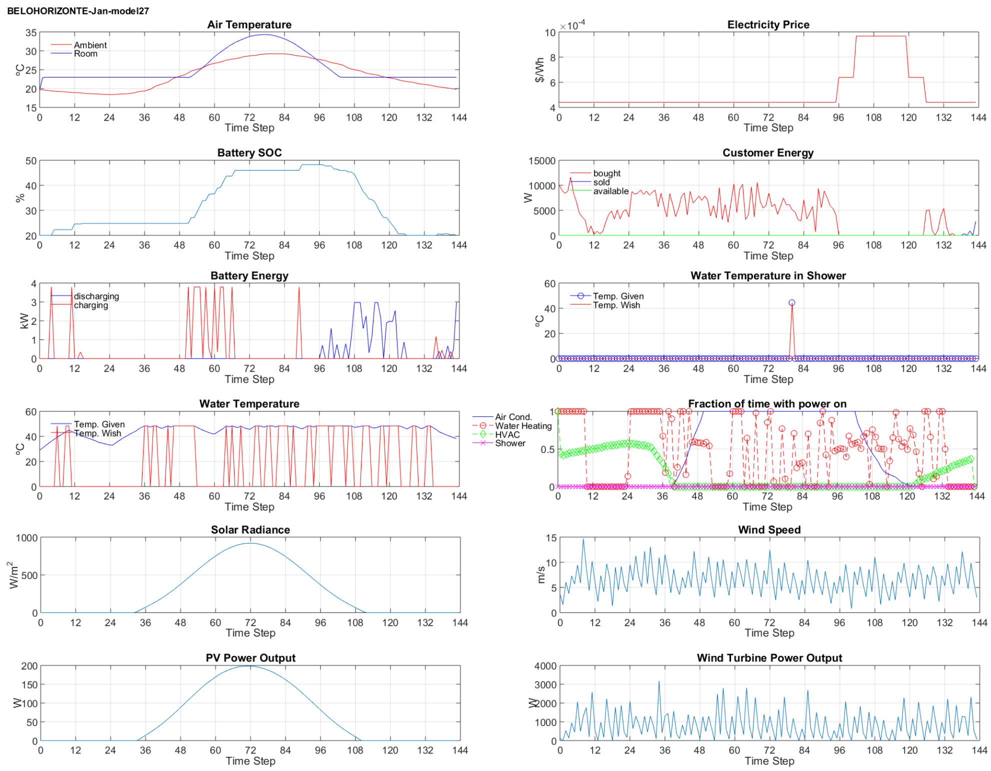

Figure 13: Results for Belo Horizonte in January.

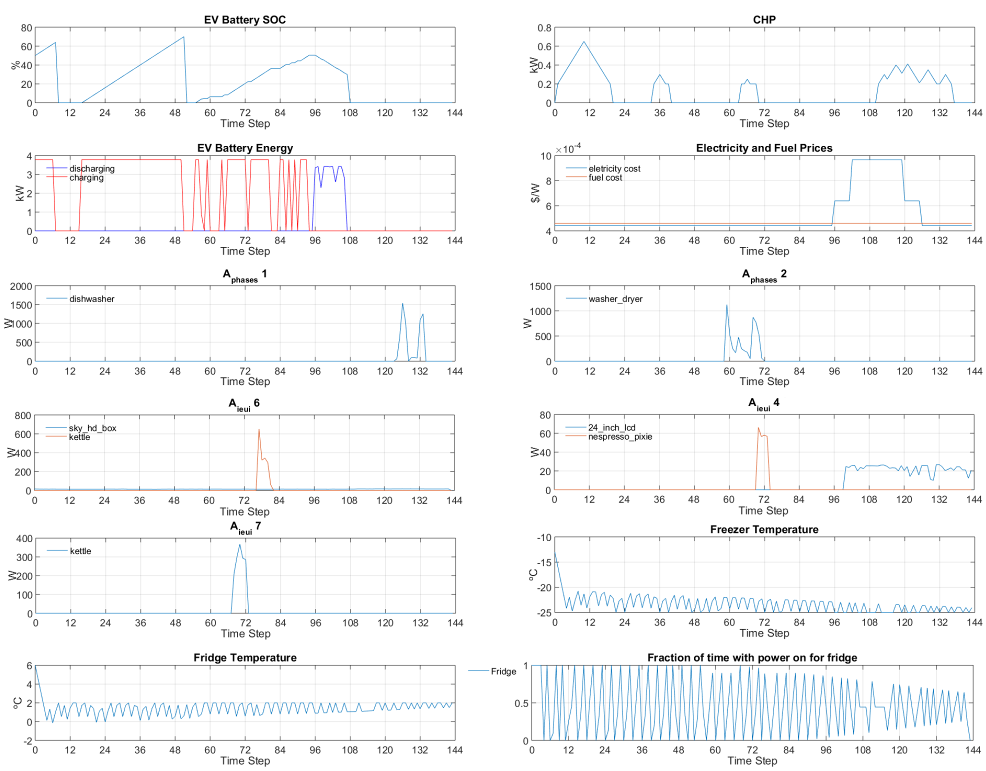

Figure 14: Results for Belo Horizonte in January.

There are 105391 constraints and 14886 variables. Around 30% of the variables are integers. CPLEX solved the problem in 36.64 s.

5 Discussion

The number of smart homes is expanding worldwide. At the same time, Energy Management system research is exploring how to use energy in an optimal way. One approach is to use optimization models of smart home appliances that are realist and efficient. This creates a trade-off between realism and complexity of modeling since to increase realism, complexity will also increase. To keep simplicity, current optimization models have limitations on the number of appliances considered and/or their reliability, decreasing the realism in the trade-off aforementioned. This paper proposes a Home Energy Management scheduling model that is accurate and that can be solved in an efficient manner with commercial solvers. First, some appliances models were proposed. Then, an extensive appliance integrated mixed integer linear optimization model that finds an optimal cost keeping a high level of user comfort is developed. For the instances considered, our model gave results that are cheaper between 8% and 389% than the compared models over a horizon of 24 hours,which means an annual savings from 544USD to 2205USD.

Appendix

A Nomenclature

Sets	
T	Time sub-intervals set for the scheduling horizon.
A	Set of electric appliances (app.).
$A_{IEUI} \subseteq A$	Set of app. with uninterruptible operation.
A^t_{IEUI}	Set of tasks from appliances $\in A_{IEUI}$.
$A^{t,a}_{IEUI} \subseteq A^t_{IEUI}$	Set of tasks from A^t_{IEUI} of the same appliance $a \in A_{IEUI}$.
$A_{Phases} \subseteq A$	Set of appliances with interruptible phases.
A^t_{Phases}	Set of tasks from appliances $a \in A_{Phases}$.
$A^{t,a}_{Phases} \subseteq A^t_{Phases}$	Set of tasks from A^t_{Phases} of the same appliance $a \in A_{Phases}$.
$A^t \in \{A^t_{Phases} \cup A^t_{IEUI}\}$	Set of appliances tasks.
D_{air}	Set of durations for hot or cold air needs.
D_{wh}	Set of durations for hot water needs.
D_{chu}	Set of durations for shower needs.
Ξ	Set of all variables in the problem.
B	Set of blocks in IBR.
Constants	
H	Number of hours in the scheduling horizon (hours).
$\Delta t_2 = H/\|T\|$	Duration of each time sub-interval (hours).
$\Delta t = 60\Delta t_2$	duration of each time slot (minutes).
	Suppose that t is an index to represent a sub-interval of time and we want to analyze $H = 24$ hours. If we cut this day in 2 sub-intervals, so, $\Delta t = 12$, $\|T\| = 2$, $t \in T = \{1, 2\}$, where $t = 1$ represent the interval time between 00:00h to 11:59h and $t = 2$ represent the remain daily hours.
w_u	Starting time discomfort weight factor. (1/h)
w_c	Weight factor for the cost (1/$).
w_t	Weight factor for the temperature discomfort (1/^{o}C).
λ^t	Energy consumption price from grid at $t \in T$ ($/Wh).
ν^t	Energy selling price to grid at $t \in T$ ($/Wh).
E^t_{pv}	Power from photovoltaic panels at $t \in T$ (W).
E^t_{wt}	Power from wind turbines at $t \in T$ (W).
E^t_{th}	Grid power capacity at sub-interval $t \in T$ (W).
E_bl^i	Energy consumption limit of block $i \in B$ (Wh).
ϖ^i	Discount to stay in block $i \in B$ (%).
S_a	Desirable task starting time of $a \in A^t$ (h).
DS_a	Bearable deadline to start task $a \in A^t$ (h).
F_a	Desirable finishing time for task $a \in A^t$ (h).
DF_a	Bearable deadline to finish task $a \in A^t$ (h).

D_a	Usage duration for task $a \in A^t_{IEUI}$ (h).
P^h_a	Fixed power of task $a \in A^t_{IEUI}$ at interval h of his load profile (W).
$P^h_{a,p}$	Fixed power for phase p of task $a \in A^t_{Phases}$ at interval h of his load profile (W).
$D_{a,p}$	Usage duration for phase p of task $a \in A^t_{Phases}$ (h).
PH_a	Number of phases of task $a \in A^t_{Phases}$.
T^t_o	Ambient temperature at sub-interval $t \in T$ (^{o}C).
T^t_f	Desirable inside air temperature at $t \in T$ (^{o}C).
$P_{heating}$	Rated power for heating machine (W).
P_{cool}	Rated power for air-conditioner (W).
ρ_{air}	Air density (kg/m^3).
V_{house}	Volume of the house (m^3).
C_{air}	Heat capacity (J/kg^{o}C).
A_{wall}	Area of the wall (m^2).
$A_{ceiling}$	Area of the ceiling (m^2).
A_{window}	Area of the window (m^2).
R_{wall}	Heat resistance of the wall (m^2 ^{o}C.h/J).
$R_{ceiling}$	Heat resistance of the ceiling (m^2 ^{o}C.h/J).
R_{window}	Heat resistance of the window (m^2 ^{o}C.h/J).
n_{ac}	Number of air changes (1/h).
$SHGC$	Solar Heat Gain Coefficient average.
H^t_{sun}	Solar radiation heat power at sub-interval t (W/m^2).
$P^t_{activity}$	Human activity metabolic rates at $t \in T$ (W/m^2).
A_{body}	Person's body area inside the home (m^2).
V_{tank}	Volume of the Water Heater (WH) (dcm^3).
P_{wh}	Rated power for WH (W).
fr^t_{wh}	Hot water flow rate for WH at $t \in T$ (l/m).
T^{wh}_f	Preferable temperature for hot water (^{o}C).
T^t_{in}	Water temperature from solar collector at $t \in T$ (^{o}C).
$(UA)_{wh}$	Loss coefficient area product for WH ($W/^oC$).
$C_p = (4190J/kg^oC)$	Thermal capacity.
T^{max}	Maximal temperature for water (^{o}C).
E_{wh}	Binary to inform if water heater exists or not.
P_{chu}	Rated power for shower resistance (W).
fr^t_{chu}	Hot water flow rate for shower at $t \in T$ (l/min).
$C_e = (4190J/kg^oC)$	Water specific heat.
T^t_{inlet}	Street water temperature at $t \in T$ (^{o}C).
T^{chu}_f	Preferable temperature for water in shower (^{o}C).
E_{bat}	Battery capacity (kWh).
SOC_{max}	Maximum battery SOC without float loss (%).
SOC_{min}	Minimum battery SOC (%).
P^{ch}_{max}	Battery maximum charging power (kW).
P^{dch}_{max}	Battery maximum discharging power(kW).
P^{ch}_{min}	Battery minimum charging power (kW).
P^{dch}_{min}	Battery minimum discharging power(kW).
η^{ch}	Inverter battery's charging efficiency.
η^{dch}	Inverter battery's discharging efficiency.
μ	Battery's charging/discharging efficiency.
p_{loss}	Battery's power float loss (kW).
$T^{start}_{freezer}$	Initial freezer temperature (^{o}C).
T^{start}_{refri}	Initial fridge temperature (^{o}C).
P_{comp}	Rated power for fridge's compressor machine (W).
T^{refri}_f	Preferable fridge compartment temperature (^{o}C).
$T^{freezer}_f$	Preferable freezer compartment temp. (^{o}C).
EV_{bat}	EV battery capacity (kWh).
$EVSOC_{max}$	Maximum EV battery SOC (%).
$EVSOC_{min}$	Minimum of EV battery SOC (%).
EVP^{ch}_{max}	EV battery maximum charging power (kW).
EVP^{dch}_{max}	EV battery maximum discharging power(kW).
EVP^{ch}_{min}	EV battery minimum charging power (kW).
EVP^{dch}_{min}	EV battery minimum discharging power(kW).

$EV\eta^{ch}$	Inverter EV battery's charging efficiency.
$EV\eta^{dch}$	Inverter EV battery's discharging efficiency.
$EV\mu$	EV battery's charging/discharging efficiency.
EVp_{loss}	EV battery's power float loss (kW).
n_{trip}	Number of complete trips in the day.
t^s_{start}	Step time in which the EV arrives at home on trip s. The EV arrives at the end of the period.
t^s_{end}	Step time in which the EV leaves the home for trip s. The EV leaves at the beginning of period.
km^{100}	Car autonomy with SOC equals to 100% (km).
$EVSOC^{end}_{min}$	Minimal SOC when EV leaves home (%).
$cons\_gas$	Distance attained by one liter of fuel (km/l).
$price\_gas$	Fuel price per liter ($/l)
$P_{gas} = \frac{price\_gas}{consu\_gas}$	Fuel price per km wheeled ($/km).
$EVSOC_{ret}$	Forecasted SOC when EV arrives. (%)
$EVSOC\_last\_day$	EV battery SOC at $t = 0$. (%)
Km^s_{next}	Distance forecasted to next trip s (km).
$rate^{fuel}_{CHP}$	Fuel price per kWh for CHP (l/kWh).
$price^{on}_{CHP}$	CHP start up cost ($).
d^{on}_{CHP}	CHP minimal duration to be on if turned on (min).
d^{off}_{CHP}	CHP minimal duration to be off if turned off (min).
nb^{η}_{CHP}	Number of parts in the overall efficiency piecewise function.
$P^{k,\eta}_{CHP,min}\ \forall\ k = \{1..nb^{\eta}_{CHP}\}$	Minimal power at breakpoint k in CHP piecewise linear overall efficiency function (kW).
$P^{k,\eta}_{CHP,max}\ \forall\ k = \{1..nb^{\eta}_{CHP}\}$	Maximal power at breakpoint k in CHP piecewise linear overall efficiency function (kW).
$\eta^k_{CHP,p}\ \forall\ k = \{1..nb^{\eta}_{CHP}\}$	Image at breakpoint k in CHP piecewise linear overall efficiency function (%).
nb^{μ}_{CHP}	Number of parts in the electrical generation efficiency piecewise function.
$P^{k,\mu}_{CHP,min}\ \forall\ k = \{1..nb^{\mu}_{CHP}\}$	Minimal power at breakpoint k in CHP piecewise linear electrical generation efficiency function (kW).
$P^{k,\mu}_{CHP,max}\ \forall\ k = \{1..nb^{\mu}_{CHP}\}$	maximal power at breakpoint k in CHP piecewise linear electrical generation efficiency function (kW).
$\mu^k_{CHP,p}\ \forall\ k = \{1..nb^{\mu}_{CHP}\}$	Image at breakpoint k in CHP piecewise linear electrical generation efficiency function (%).
r^{down}_{CHP}	Maximum ramp down for CHP (kW/min).
r^{up}_{CHP}	Maximum ramp up for CHP (kW/min).
$P_{KW} = rate^{fuel}_{CHP} \times price\_gas$	CHP price per kW ($/kWh).
$y^{last\_day}_{CHP}$	Binary to determine if CHP is on or off at $t = 0$.
$\bar{\eta}$	Overall efficiency average.
$\bar{\mu}$	Electrical generation efficiency average.
y^{ini}_{CHP}	Initial value for variable y_{CHP}.
P^{ini}_{CHPe}	Initial value for variable P_{CHPe} (kW).

Variables

C^t	Monetary cost at $t \in T$ ($).
E^t_g	Fixed power took from the grid at $t \in T$ (W).
E^t_v	Fixed power injected into the grid at $t \in T$ (W).
x^t_a	Fixed power consumption of appliance a at $t \in T$(W).
E^t_{av}	Fixed power credit available at $t \in T$ (W).
V^t_a	Temperature discomfort due target temperature deviation of appliance a at $t \in T$ (^{o}C).
U^t_a	Time discomfort due deviation from target time of use for appliance a at $t \in T$ (h).
ζ_a	Discomfort of not doing the task $a \in A^t_{IEUI}$.
$\Psi_{a,p}$	Discomfort of not doing phase p of task $a \in A^t_{Phases}$.
$P^{ch,t}_{bat}$	Charging power of battery (kW).
$P^{dch,t}_{bat}$	Discharging power of battery (kW).
$y^{ch,t}_{bat}$	On/off binary for battery charging at $t \in T$.
$y^{dch,t}_{bat}$	On/off binary for battery discharging at $t \in T$.
SOC^t	Battery's state of charge at sub-interval t (%).
y^t_{float}	Binary to activate battery float losses at $t \in T$.
T^t_{room}	Room temperature at sub-interval $t \in T$ (^{o}C).
y^t_{HVAC}	On/off binary for heating operation at $t \in T$.
y^t_{air}	On/off binary for air-conditioner operation at $t \in T$.
z^t_{air}	Fraction of Δ_t in $t \in T$ in which air-conditioner is on.
z^t_{HVAC}	Fraction of Δ_t in $t \in T$ in which heating is on.
$T^t_{out,wh}$	Water heater output temperature at $t \in T$ (^{o}C).
y^t_{wh}	On/off binary for water heater operation at $t \in T$.

$T^t_{chu\_hand}$	Shower water temperature manually adjusted at sub-interval t (^{o}C).
$T^t_{out,chu}$	Shower output water temperature at $t \in T$ (^{o}C).
$y^t_{chu,hot}$	On/off binary for shower operation at $t \in T$.
$T^t_{freezer}$	Freezer temperature at sub-interval t (^{o}C).
T^t_{refri}	Fridge temperature at sub-interval t (^{o}C).
y^t_{comp}	On/off binary for fridge's compressor at $t \in T$.
y^t_a	Binary that indicates whether the operation of task $a \in A^t_{IEUI}$ starts at sub-interval t.
$y_{a,b}$	Binary that indicates if task $a \in A^t_{IEUI}$ has to be done after task $b \in A^t_{IEUI}$ be finished.
$y^t_{a,p}$	Binary that indicates whether the operation of phase p of task $a \in A^t_{Phases}$ starts at sub-interval t.
$y^p_{a,b}$	Binary that indicates if task $a \in A^t_{Phases}$ has to be done after task $b \in A^t_{Phases}$ be finished.
C_{ev}	Fuel cost used in the electric vehicle (EV) (\$).
$P^{ch,t}_{EVbat}$	Charging power of EV battery (kW).
$P^{dch,t}_{EVbat}$	Discharging power of EV battery (kW).
$y^{ch,t}_{EVbat}$	On/off binary for EV battery charging at $t \in T$.
$y^{dch,t}_{EVbat}$	On/off binary for EV battery discharging at $t \in T$.
$EVSOC^t$	EV battery's state of charge at $t \in T$ (%).
$y^t_{EVfloat}$	Binary to start EV battery float losses at $t \in T$.
Km^s_{fuel}	Amount of Km from trip s using fuel (km).
C^s_{ev}	Cost related to the fuel used in trip s (\$).
C^t_{CHP}	CHP cost operation at sub-interval $t \in T$ (\$).
P^t_{CHPe}	CHP electrical power output at $t \in T$ (KW).
P^t_{CHPt}	CHP thermal power output at $t \in T$ (KW).
$P^t_{CHP,fuel}$	CHP power input from fuel at $t \in T$ (KW).
y^t_{CHP}	On/off binary for CHP operation at $t \in T$.
z^t_{CHP}	Binary to determine if CHP is turned on at $t \in T$.
zd^t_{CHP}	Binary to determine if CHP is turned off at $t \in T$.
w^t_{up}	Fraction of Δ_t in $t \in T$ in which CHP ramps up.
w^t_{down}	Fraction of Δ_t in $t \in T$ in which CHP ramps down.
$E^{t,i}_g$	Fixed power took from the grid at $t \in T$ from block $i \in B$ (W).
y^i_g	Binary to determine if block $i \in B$ is selected or not.

B Auxiliary Equations

$$1000(p^{ch,t}_{EVbatt} + P^{ch,t}_{bat}) + \sum_{a\in A} x^t_a + E^t_{av} = E^{t-1}_{av} + E^t_{wt} + E^t_{pv} + \sum_{i\in B} E^{t,i}_g + 1000(p^{dch,t}_{EVbatt} + P^{dch,t}_{bat} + P^t_{CHPe}) \ \forall\, t \in T \quad (147)$$

C Temperature refrigerator equations

$$\begin{aligned} T^t_{eq,f} &= \frac{(UA_f + \dot m_{d,f} c_{pa}) T^t_a + UA_m T^t_r + \frac{r \dot m_a c_{pa}}{3600}(T_{newton} y^t_{comp} + (\kappa)(1 - y^t_{comp}) + \frac{3600 w_{fan}}{\dot m_a C_{p,a}} y^t_{comp}) y^t_{comp}}{UA_f + UA_m + \dot m_d C_{p,a} + \frac{\dot m_f C_{p,a}}{3600} y^t_{comp}} \\ &= \frac{(UA_f + \dot m_{d,f} c_{pa}) T^t_a + UA_m T^t_r + \frac{r \dot m_a c_{pa}}{3600}(T_{newton} y^t_{comp} + \frac{3600 w_{fan}}{\dot m_a C_{p,a}} y^t_{comp})}{UA_f + UA_m + \dot m_d C_{p,a} + \frac{\dot m_f C_{p,a}}{3600} y^t_{comp}} \text{ because } (y^t_{comp})^2 = y^t_{comp} \end{aligned} \quad (148)$$

$$
\begin{aligned}
T_{eq,r} &= \frac{(UA_r+\dot{m}_{d,r}c_{pa})T_a^t+UA_mT_f^t+\frac{(1-r)\dot{m}_a c_{pa}}{3600}(T_{newton}y_{comp}^t+(\kappa)(1-y_{comp}^t)+\frac{3600w_{fan}}{\dot{m}_a C_{p,a}}y_{comp}^t)y_{comp}^t}{UA_r+UA_m+\dot{m}_dC_{p,a}+\frac{\dot{m}_rC_{p,a}}{3600}y_{comp}^t} \\
&= \frac{(UA_r+\dot{m}_{d,r}c_{pa})T_a^t+UA_mT_f^t+\frac{(1-r)\dot{m}_a c_{pa}}{3600}(T_{newton}y_{comp}^t+\frac{3600w_{fan}}{\dot{m}_a C_{p,a}}y_{comp}^t)}{UA_r+UA_m+\dot{m}_dC_{p,a}+\frac{\dot{m}_rC_{p,a}}{3600}y_{comp}^t} \text{ because } (y_{comp}^t)^2 = y_{comp}^t
\end{aligned} \tag{149}
$$

References

[1] Christopher O. Adika and Lingfeng Wang. Autonomous appliance scheduling for household energy management. IEEE Transactions on Smart Grid, 5(2):673–682, 2014.

[2] Christopher O. Adika and Lingfeng Wang. Smart charging and appliance scheduling approaches to demand side management. International Journal of Electrical Power & Energy Systems, 57:232–240, 2014.

[3] Alessandro Agnetis, Gianluca de Pascale, Paolo Detti, and Antonio Vicino. Load scheduling for household energy consumption optimization. IEEE Transactions on Smart Grid, 4(4):2364–2373, 2013.

[4] Refrigerating American Society of Heating and Inc. Air-Conditioning Engineers. 2013 ASHRAE Handbook - Fundamentals (SI Edition). 2013.

[5] Refrigerating American Society of Heating and Inc. Air-Conditioning Engineers. 2015 ASHRAE HANDBOOK Heating, Ventilating, and Air-Conditioning APPLICATIONS (SI Edition). 2015.

[6] ANEEL. Matriz de energia elétrica. accessed Dec. 2017.

[7] Amjad Anvari-Moghaddam, Hassan Monsef, and Ashkan Rahimi-Kian. Cost-effective and comfort-aware residential energy management under different pricing schemes and weather conditions. Energy and Buildings, 86:782–793, 2015.

[8] Amjad Anvari-Moghaddam, Hassan Monsef, and Ashkan Rahimi-Kian. Optimal smart home energy management considering energy saving and a comfortable lifestyle. IEEE Transactions on Smart Grid, 6(1):324–332, 2015.

[9] A. Arabali, M. Ghofrani, M. Etezadi-Amoli, M. S. Fadali, and Y. Baghzouz. Genetic-algorithm-based optimization approach for energy management. IEEE Transactions on Power Delivery, 28(1):162–170, 2013.

[10] Sean Barker, Sandeep Kalra, David Irwin, and Prashant Shenoy. Empirical characterization and modeling of electrical loads in smart homes. 2013 International Green Computing Conference (IGCC), pages 1–10, 2013.

[11] Marc Beaudin and Hamidreza Zareipour. Home energy management systems: A review of modelling and complexity. Renewable and Sustainable Energy Reviews, 45:318–335, 2015.

[12] Bruno N. Borges. Modelagem semi-empírica de um refrigerador frost-free sujeito a abertura de portas. 2013. Thesis, Universidade Federal de Santa Catarina, Florianópolis, 2013.

[13] Bruno N. Borges, Christian J. L. Hermes, Joaquim M. Gonçalves, and Cláudio Melo. Transient simulation of household refrigerators: A semi-empirical quasi-steady approach. Applied Energy, 88(3):748–754, 2011.

[14] Brazil. Lei n^o 12.212, de 20 de janeiro de 2010, 2010. accessed Dec. 2017.

[15] M. Castillo-Cagigal, E. Caamaño-Martín, E. Matallanas, D. Masa-Bote, A. Gutiérrez, F. Monasterio-Huelin, and J. Jiménez-Leube. PV self-consumption optimization with storage and active DSM for the residential sector. Solar Energy, 85(9):2338–2348, 2011.

[16] Cemig. Cities of the future project. accessed Dec. 2017.

[17] Chen Chen, Jianhui Wang, Yeonsook Heo, and Shalinee Kishore. MPC-based appliance scheduling for residential building energy management controller. IEEE Transactions on Smart Grid, 4(3):1401–1410, 2013.

[18] Xiaodao Chen, Tongquan Wei, and Shiyan Hu. Uncertainty-aware household appliance scheduling considering dynamic electricity pricing in smart home. IEEE Transactions on Smart Grid, 4(2):932–941, 2013.

[19] Zhi Chen, Lei Wu, and Yong Fu. Real-time price-based demand response management for residential appliances via stochastic optimization and robust optimization. IEEE Transactions on Smart Grid, 3(4):1822–1831, 2012.

[20] Nicos Christofides, R. Alvarez-Valdes, and J. M. Tamarit. Project scheduling with resource constraints: A branch and bound approach. European Journal of Operational Research, 29(3):262–273, 1987.

[21] Gregory Chagas da Costa Gomes. Avaliação do comportamento de refrigeradores domésticos frente a defeitos provocados e emulados. Thesis, Universidade Federal de Santa Catarina, 2015.

[22] Alessandro José da Silva, Carlos Roberto Costa Nascimento, Leandro Ferreira da Silva, and Taíza de Pinho Barroso Lucas. Análise topoclimática em unidade de conservação urbana a partir da temperatura e umidade relativa do ar. e-Scientia, 4(1):21–30, 2011.

[23] Michel De Lara, Pierre Carpentier, Jean-Philippe Chancelier, and Vincent Leclere. Optimization methods for the smart grid. Report commissioned by the Conseil Français de l'Energie, Ecole des Ponts ParisTech, 2014.

[24] W. De Soto, S. A. Klein, and W. A. Beckman. Improvement and validation of a model for photovoltaic array performance. Solar Energy, 80(1):78–88, 2006.

[25] Ruilong Deng, Zaiyue Yang, Jiming Chen, and Mo-Yuen Chow. Load scheduling with price uncertainty and temporally-coupled constraints in smart grids. IEEE Transactions on Power Systems, 29(6):2823–2834, 2014.

[26] William B. DeOreo, Peter W. Mayer, Benedykt Dziegielewski, and Jack Kiefer. Residential end uses of water, version 2. Water Research Foundation, 2016.

[27] Katia Gregio Di Santo, Eduardo Kanashiro, Silvio Giuseppe Di Santo, and Marco Antonio Saidel. A review on smart grids and experiences in brazil. Renewable and Sustainable Energy Reviews, 52:1072–1082, 2015.

[28] Pengwei Du and Ning Lu. Appliance commitment for household load scheduling. IEEE Transactions on Smart Grid, 2(2):411–419, 2011.

[29] John A Duffie and William A Beckman. Solar Engineering of Thermal Processes, volume 4. Wiley New York, 2013.

[30] Mohamed E. El-hawary. The smart grid—state-of-the-art and future trends. Electric Power Components and Systems, 42(3–4):239–250, 2014.

[31] Energética, Empresa de Pesquisa. Plano Nacional de Energia 2030. Rio de Janeiro, 2007.

[32] Ozan Erdinc, Nikolaos G. Paterakis, Tiago D. P. Mendes, Anastasios G. Bakirtzis, and Joao P. S. Catalao. Smart household operation considering bi-directional EV and ESS utilization by real-time pricing-based DR. IEEE Transactions on Smart Grid, 6(3):1281–1291, 2015.

[33] M. Erol-Kantarci and H. T. Mouftah. Wireless sensor networks for cost-efficient residential energy management in the smart grid. IEEE Transactions on Smart Grid, 2(2):314–325, 2011.

[34] M. Fadaeenejad, A. M. Saberian, Mohd Fadaee, M. A. M. Radzi, H. Hizam, and M. Z. A. AbKadir. The present and future of smart power grid in developing countries. Renewable and Sustainable Energy Reviews, 29:828–834, 2014.

[35] Mohammad Ali Fotouhi Ghazvini, João Soares, Omid Abrishambaf, Rui Castro, and Zita Vale. Demand response implementation in smart households. Energy and Buildings, 143:129–148, 2017.

[36] Sajjad Golshannavaz. Cooperation of electric vehicle and energy storage in reactive power compensation: An optimal home energy management system considering PV presence. Sustainable Cities and Society, 39:317–325, 2018.

[37] Sebastian Gottwalt, Wolfgang Ketter, Carsten Block, John Collins, and Christof Weinhardt. Demand side management—A simulation of household behavior under variable prices. Energy Policy, 39(12):8163–8174, 2011.

[38] A. D. Hawkes, D. J. L. Brett, and N. P. Brandon. Fuel cell micro-CHP techno-economics: Part 1 – Model concept and formulation. International Journal of Hydrogen Energy, 34(23):9545–9557, 2009.

[39] A. D. Hawkes, D. J. L. Brett, and N. P. Brandon. Fuel cell micro-CHP techno-economics: Part 2 – Model application to consider the economic and environmental impact of stack degradation. International Journal of Hydrogen Energy, 34(23):9558–9569, 2009.

[40] Ying-Yi Hong, Jie-Kai Lin, Ching-Ping Wu, and Chi-Cheng Chuang. Multi-objective air-conditioning control considering fuzzy parameters using immune clonal selection programming. IEEE Transactions on Smart Grid, 3(4):1603–1610, 2012.

[41] Tanguy Hubert and Santiago Grijalva. Modeling for residential electricity optimization in dynamic pricing environments. IEEE Transactions on Smart Grid, 3(4):2224–2231, 2012.

[42] Anders Frick Johan Fagerberg. Smart homes and home automation. Technical report, Berg Insight, 2015.

[43] Jack Kelly and William Knottenbelt. The UK-DALE dataset, domestic appliance-level electricity demand and whole-house demand from five UK homes. Scientific Data, 2:150007, 2015.

[44] Tùng T. Kim and H. Vincent Poor. Scheduling power consumption with price uncertainty. IEEE Transactions on Smart Grid, 2(3):519–527, 2011.

[45] Phillip Oliver Kriett and Matteo Salani. Optimal control of a residential microgrid. Energy, 42(1):321–330, 2012.

[46] Jang-Won Lee and Du-Han Lee. Residential electricity load scheduling for multi-class appliances with time-of-use pricing. pages 1194–1198., 2011.

[47] Andréa P. Leite, Djalma M. Falcão, and Carmen L.T. Borges. Modelagem de usinas eólicas para estudos de confiabilidade. Sba: Controle & Automação Sociedade Brasileira de Automatica, 17:177–188, 2006.

[48] Benoît Lévesque, Michel Lavoie, and Jean Joly. Residential water heater temperature: 49 or 60 degrees celsius? The Canadian Journal of Infectious Diseases, 15(1):11–12, 2004.

[49] F. Y. Melhem, O. Grunder, Z. Hammoudan, and N. Moubayed. Optimization and energy management in smart home considering photovoltaic, wind, and battery storage system with integration of electric vehicles. Cana-

dian Journal of Electrical and Computer Engineering-Revue Canadienne De Genie Electrique Et Informatique, 40(2):128–138, 2017.

[50] Henrique Leão de Sá Menezes. Avaliação da aplicação da modalidade tarifária horária branca: Estudo de caso para consumidores residenciais. Report, Universidade de Brasília, 2015.

[51] Ministério de Minas e Energia. Projeção da demanda de energia elétrica para os próximos 5 anos (2016-2020). NOTA TÉCNICA DEA 19/15, 2015.

[52] Amin Mohseni, Seyed Saeidollah Mortazavi, Ahmad Ghasemi, Ali Nahavandi, and Masoud Talaei abdi. The application of household appliances' flexibility by set of sequential uninterruptible energy phases model in the day-ahead planning of a residential microgrid. Energy, 139:315–328, 2017.

[53] Amir-Hamed Mohsenian-Rad and Alberto Leon-Garcia. Optimal residential load control with price prediction in real-time electricity pricing environments. IEEE Transactions on Smart Grid, 1(2):120–133, 2010.

[54] Chukwuka G. Monyei, Aderemi O. Adewumi, Daniel Akinyele, Olubayo M. Babatunde, Michael O. Obolo, and Joshua C. Onunwor. A biased load manager home energy management system for low-cost residential building low-income occupants. Energy, 150:822–838, 2018.

[55] Afshin Najafi-Ghalelou, Sayyad Nojavan, and Kazem Zare. Heating and power hub models for robust performance of smart building using information gap decision theory. International Journal of Electrical Power & Energy Systems, 98:23–35, 2018.

[56] Duong Tung Nguyen and Long Bao Le. Joint optimization of electric vehicle and home energy scheduling considering user comfort preference. IEEE Transactions on Smart Grid, 5(1):188–199, 2014.

[57] Hieu T Nguyen, Duong T Nguyen, and Long B Le. Energy management for households with solar assisted thermal load considering renewable energy and price uncertainty. IEEE Transactions on Smart Grid, 6(1):301–314, 2015.

[58] Xuan Hieu Nguyen and Minh Phuong Nguyen. Mathematical modeling of photovoltaic cell/module/arrays with tags in Matlab/Simulink. Environmental Systems Research, 4(1), 2015.

[59] NISSAN. Nissan Leaf presentation. accessed Dec. 2017.

[60] Nikolaos G. Paterakis, Ozan Erdinc, Anastasios G. Bakirtzis, and Joao P. S. Catalao. Optimal household appliances scheduling under day-ahead pricing and load-shaping demand response strategies. IEEE Transactions on Industrial Informatics, 11(6):1509–1519, 2015.

[61] Michael Angelo A. Pedrasa, Ted D. Spooner, and Iain F. MacGill. Coordinated scheduling of residential distributed energy resources to optimize smart home energy services. IEEE Transactions on Smart Grid, 1(2):134–143, 2010.

[62] Michael Angelo A. Pedrasa, Ted D. Spooner, and Iain F. MacGill. A novel energy service model and optimal scheduling algorithm for residential distributed energy resources. Electric Power Systems Research, 81(12):2155–2163, 2011.

[63] Manisa Pipattanasomporn, Murat Kuzlu, Saifur Rahman, and Yonael Teklu. Load profiles of selected major household appliances and their demand response opportunities. IEEE Transactions on Smart Grid, 5(2):742–750, 2014.

[64] Li Ping Qian, Ying Jun Angela Zhang, Jianwei Huang, and Yuan Wu. Demand response management via real-time electricity price control in smart grids. IEEE Journal on Selected Areas in Communications, 31(7):1268–1280, 2013.

[65] Mohammad Rastegar, Mahmud Fotuhi-Firuzabad, and Farrokh Aminifar. Load commitment in a smart home. Applied Energy, 96:45–54, 2012.

[66] Ian Richardson, Murray Thomson, David Infield, and Conor Clifford. Domestic electricity use: A high-resolution energy demand model. Energy and Buildings, 42(10):1878–1887, 2010.

[67] E. M. G. Rodrigues, R. Godina, E. Pouresmaeil, J. R. Ferreira, and J. P. S. Catalão. Domestic appliances energy optimization with model predictive control. Energy Conversion and Management, 142:402–413, 2017.

[68] Hee-Tae Roh and Jang-Won Lee. Residential demand response scheduling with multiclass appliances in the smart grid. IEEE Transactions on Smart Grid, 7(1):94–104, 2016.

[69] Ameena Saad al sumaiti, Mohammed Hassan Ahmed, and Magdy M. A. Salama. Smart home activities: A literature review. Electric Power Components and Systems, 42(3–4):294–305, 2014.

[70] Miadreza Shafie-Khah and Pierluigi Siano. A stochastic home energy management system considering satisfaction cost and response fatigue. IEEE Transactions on Industrial Informatics, 14(2):629–638, 2018.

[71] Mohammad Shakeri, Mohsen Shayestegan, Hamza Abunima, S. M. Salim Reza, M. Akhtaruzzaman, A. R. M. Alamoud, Kamaruzzaman Sopian, and Nowshad Amin. An intelligent system architecture in home energy management systems (HEMS) for efficient demand response in smart grid. Energy and Buildings, 138:154–164, 2017.

[72] Shengnan Shao, Manisa Pipattanasomporn, and Saifur Rahman. Development of physical-based demand response-enabled residential load models. IEEE Transactions on Power Systems, 28(2):607–614, 2013.

[73] Elham Shirazi and Shahram Jadid. Cost reduction and peak shaving through domestic load shifting and DERs. Energy, 124:146–159, 2017.

[74] Elham Shirazi, Alireza Zakariazadeh, and Shahram Jadid. Optimal joint scheduling of electrical and thermal appliances in a smart home environment. Energy Conversion and Management, 106:181–193, 2015.

[75] Javier Silvente and Lazaros G. Papageorgiou. An MILP formulation for the optimal management of microgrids with task interruptions. Applied Energy, 206:1131–1146, 2017.

[76] T. Sousa, H. Morais, Z. Vale, P. Faria, and J. Soares. Intelligent energy resource management considering vehicle-to-grid: A simulated annealing approach. IEEE Transactions on Smart Grid, 3(1):535–542, 2012.

[77] L. Stankovic, V. Stankovic, J. Liao, and C. Wilson. Measuring the energy intensity of domestic activities from smart meter data. Applied Energy, 183:1565–1580, 2016.

[78] Roland Stull. Practical Meteorology: An Algebra Based Survey of Atmospheric Science. BC Campus, 2016.

[79] Dimitrios Thomas, Olivier Deblecker, and Christos S. Ioakimidis. Optimal operation of an energy management system for a grid-connected smart building considering photovoltaics' uncertainty and stochastic electric vehicles' driving schedule. Applied Energy, 210:1188–1206, 2018.

[80] George Tsagarakis, Adam Collin, and Aristides Kiprakis. A statistical survey of the UK residential sector electrical loads. International Journal of Emerging Electric Power Systems, 14(5), 2013.

[81] D. Villanueva and A. Feijóo. Wind power distributions: A review of their applications. Renewable and Sustainable Energy Reviews, 14(5):1490–1495, 2010.

[82] Chengshan Wang, Yue Zhou, Bingqi Jiao, Yamin Wang, Wenjian Liu, and Dan Wang. Robust optimization for load scheduling of a smart home with photovoltaic system. Energy Conversion and Management, 102:247–257, 2015.

[83] Zaiyue Yang, Keyu Long, Pengcheng You, and Mo-Yuen Chow. Joint scheduling of large-scale appliances and batteries via distributed mixed optimization. IEEE Transactions on Power Systems, 30(4):2031–2040, 2015.

[84] Wen Yao-Jung and Alice M. Agogino. Wireless networked lighting systems for optimizing energy savings and user satisfaction. pages 1–7, 2008.

[85] Zhe Yu, Liyan Jia, Mary C. Murphy-Hoye, Annabelle Pratt, and Lang Tong. Modeling and stochastic control for home energy management. IEEE Transactions on Smart Grid, 4(4):2244–2255, 2013.

[86] A Cengel Yunus. Heat Transfer: A Practical Approach. McGraw-Hill, New York, 2003.

[87] Bin Zhou, Wentao Li, Ka Wing Chan, Yijia Cao, Yonghong Kuang, Xi Liu, and Xiong Wang. Smart home energy management systems: Concept, configurations, and scheduling strategies. Renewable and Sustainable Energy Reviews, 61:30–40, 2016.

[88] Suyang Zhou, Zhi Wu, Jianing Li, and Xiao-ping Zhang. Real-time energy control approach for smart home energy management system. Electric Power Components and Systems, 42(3–4):315–326, 2014.

[89] Zhao Zhuang, Lee Won Cheol, Shin Yoan, and Song Kyung-Bin. An optimal power scheduling method for demand response in home energy management system. IEEE Transactions on Smart Grid, 4(3):1391–1400, 2013.